AD-A135 693 PICOSECOND LASER PULSE INTERACTIONS WITH METALLIC AND SEMICONDUCTOR SURFACES(U) HARVARD UNIV CAMBRIDGE MA DIV OF APPLIED SCIENCES N BLOEMBERGEN ET AL. 01 NOV 83 1/1

UNCLASSIFIED N00014-83-K-0030 F/G 20/12 NL

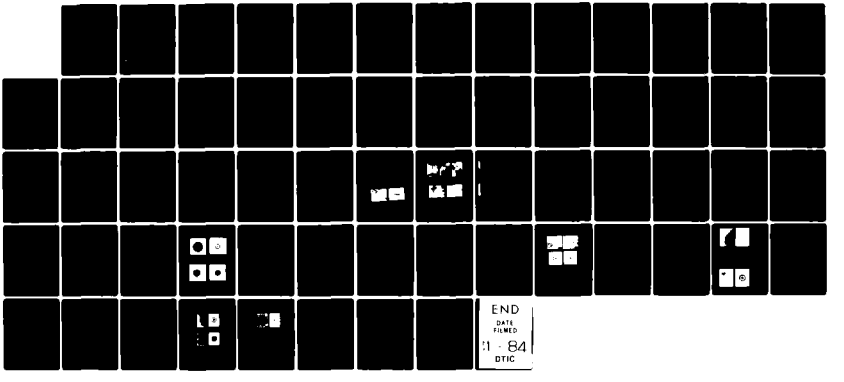

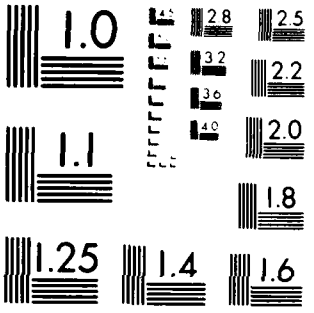

Unclassified
SECURITY CLASSIFICATION OF THIS PAGE (When Data Entered)

REPORT DOCUMENTATION PAGE

READ INSTRUCTIONS BEFORE COMPLETING FORM

1. REPORT NUMBER: Annual Progress Report No. 1	2. GOVT ACCESSION NO.
3. RECIPIENT'S CATALOG NUMBER	
4. TITLE (and Subtitle): Picosecond Laser Pulse Interactions with Metallic and Semiconductor Surfaces	5. TYPE OF REPORT & PERIOD COVERED: Annual Technical Report Nov. 1, 1982 - Oct. 31, 1983
6. PERFORMING ORG. REPORT NUMBER	
7. AUTHOR(s): Nicolaas Bloembergen and Frans Spaepen	8. CONTRACT OR GRANT NUMBER(s): N00014-83-K-0030
9. PERFORMING ORGANIZATION NAME AND ADDRESS: Division of Applied Sciences, Harvard University, Cambridge, MA 02138	10. PROGRAM ELEMENT, PROJECT, TASK AREA & WORK UNIT NUMBERS
11. CONTROLLING OFFICE NAME AND ADDRESS: Office of Naval Research, 800 N. Quincy Street, Arlington, VA 22217	12. REPORT DATE: November 1, 1983
	13. NUMBER OF PAGES: 5 + appendices
14. MONITORING AGENCY NAME & ADDRESS (if different from Controlling Office)	15. SECURITY CLASS. (of this report): Unclassified
	15a. DECLASSIFICATION, DOWNGRADING SCHEDULE

16. DISTRIBUTION STATEMENT (of this Report)

This document has been approved for public release and sale; its distribution is unlimited.

17. DISTRIBUTION STATEMENT (of the abstract entered in Block 20, if different from Report)

Approved for public release, distribution unlimited.

18. SUPPLEMENTARY NOTES

A

19. KEY WORDS (Continue on reverse side if necessary and identify by block number)

Laser-Materials Interactions, Picosecond Pulses, Metallic and Semiconductor Surfaces, Phase Transitions, Ultrafast Heating and Cooling

20. ABSTRACT (Continue on reverse side if necessary and identify by block number)

Picosecond heating and cooling experiments on silicon surfaces are reported. The surfaces are probed by a picosecond pulse, following the heating pulse, as a function of wave length, time delay and energy fluence. Picosecond laser-induced transformations of modulated metal films extend the glass formation range. New glassy alloys have been formed.

DD FORM 1 JAN 73 1473 EDITION OF 1 NOV 65 IS OBSOLETE
S/N 0102-014-6601

Unclassified
SECURITY CLASSIFICATION OF THIS PAGE (When Data Entered)

AD-A135693

DTIC FILE COPY

83 12 12 052

HARVARD UNIVERSITY
Division of Applied Sciences
Pierce Hall, 29 Oxford Street
Cambridge, Massachusetts 02138

Annual Progress Letter
ONR Contract N00014-83-K-0030
For Period: November 1, 1982 - October 31, 1983

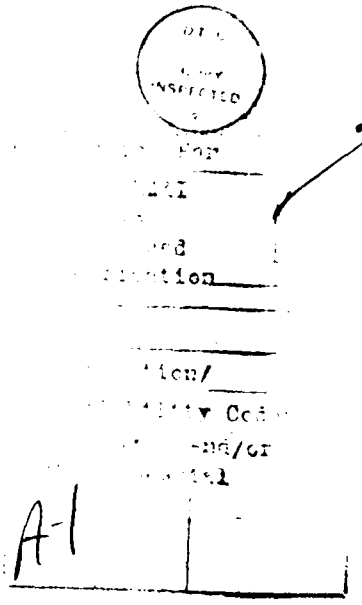

A. Picosecond Heating of Silicon

The personnel associated with this project consisted of:

Dr. N. Bloembergen, Principal Investigator

Dr. J. M. Liu

Dr. L. A. Lompre

Dr. H. Kurz

Dr. A. M. Malvezzi

During the first year of this contract we have reached many of the objectives set for picosecond pumping and probing of silicon surfaces. The samples consisted of high resistivity single-crystal wafers and silicon-on-sapphire (SOS) crystalline films with thicknesses between 0.1-0.5 μm. The reflectance and transmission of these samples was probed, after a green pump pulse at 0.53 μm of 20 ps duration had created a dense electron-hole plasma and heated the lattice. These measurements yielded the complex index of refraction at several wavelengths in the visible and infrared, at 0.53 μm, 1.06 μm, 1.9 μm and 2.8 μm. The picosecond probe pulses at the last two wavelengths were obtained by the stimulated Raman effect, as the first Stokes of H_2 gas and the second Stokes of CH_4 gas, respectively. The data were obtained as a function

of pump fluence and of the time delay following the pump pulse. The data at 0.53 μm allow a determination of the lattice temperature, which produces variations in the index of refraction for the indirect gap transition. The infrared data permit a precise determination of the plasma density. The latter never exceeds 5×10^{20} carriers/cm^3 before the silicon melts. Detailed profiles of carrier density and lattice temperature following the heating pulse are consistent with a picture in which the dense carrier gas and the lattice equilibrate to the same temperature in picoseconds or less, and in which the carrier density decays from its maximum value of less than 10^{21} /cc in about 100 ps, due to Auger recombination. A novel three-pulse experiment, in which a first pulse at 0.53 μm creates the plasma, a second pulse at 1.06 μm heats this plasma, and a third pulse at various wavelengths probes the resulting changes in index of refraction, has also been introduced.

For further details we refer to the (p)reprints of technical papers presented at international conferences or published in technical journals. These papers are attached as appendices.

These optical methods of approach to picosecond heating problems will be applied next to GaAs and germanium samples. Progress has also been made on the photoelectric emission and the emission of positive ions from silicon surfaces. This work will be continued during the next year.

List of papers supported by ONR Contract N00014-83-K-0030 and published or submitted for publication in 1983.

1. 'Picosecond time-resolved detection of plasma formation and phase transitions in silicon', J.M. Liu, H. Kurz and N. Bloembergen, in Laser-Solid Interactions and Transient Thermal Processing of Materials, W.L. Brown,

R.A. Lemons and J. Narayan, editors, Materials Research Society Symposium Proceedings, Vol. 13 (Elsevier North-Holland, New York, 1983), pp. 3-12.

2. 'Fundamentals of pulsed laser irradiation of silicon', H. Kurz, L.A. Lompre and J.M. Liu, in Proc. Materials Research Society-Europe Meeting, Laser Solid Interactions and Transient Thermal Processing of Materials, Strasbourg, May 1983, J. de Physique, Colloques (1983).

3. 'Time-resolved temperature measurement of picosecond laser irradiated silicon', L.A. Lompre, J.M. Liu, H. Kurz and N. Bloembergen, Appl. Phys. Lett. 43, 168-170 (1983).

4. 'Optical heating of electron-hole plasma in silicon by picosecond pulses', L.A. Lompre, J.M. Liu, H. Kurz and N. Bloembergen, Appl. Phys. Lett. (accepted for publication, 1984).

5. 'Picosecond time-resolved reflectivity and transmission at 1.9 and 2.8 μm of laser-generated plasmas in silicon and germanium', H.M. van Driel, L.A. Lompre and N. Bloembergen, Appl. Phys. Lett. (accepted for publication).

B. Picosecond Pulsed Laser Induced Transformations in Metals and Alloys

The personnel associated with this effort were:

F. Spaepen, Principal Investigator

C.-J. Lin, Graduate Student

C. A. MacDonald, Graduate Student

We have studied a variety of binary alloys, and found the following

transformation products:

Fe-B:	0- 4%B:	supersaturated b.c.c.
	5- 18%B:	glass
	In conventional glass formation (melt-spinning), minimum of 12%B required.	
Ni-Nb:	0- 18%Ni:	supersaturated b.c.c.
	23- 82%Ni:	glass
	89-100%Ni:	supersaturated f.c.c. (heavily-faulted with twins and stacking faults)
	The conventional glass formation range is 40-70%Ni	
Co-Nb:	60%Co:	glass
Co-Mo:	45%Co:	glass
Mo-Ni:	30, 50 60%Ni:	glass
Co-Cu:	50%Cu:	supersaturated f.c.c.
Au-Co:	40%Co:	supersaturated f.c.c.
	60, 70%Co:	mixture of supersaturated f.c.c. and glass

Using picosecond laser quenching, the glass formation range has been greatly extended beyond that for conventional quenching, and a number of new glasses have been formed. The only metals that could not be quenched into glasses were: pure or dilute metals, and alloys for which the crystal competing with glass formation was disordered f.c.c. (Cu-Co).

In pure metals, such as Fe, very high crystal regrowth speeds (at least 500m/sec) were inferred from the growth of crystals to a diameter, parallel to the surface, as large as several μm.

In marginally glass forming alloys, such as Fe-4%B, interfacial instabilities were observed in the latter stages of solidification, resulting in a crystalline-amorphous two-phase morphology.

We have started a study aimed at direct measurements of crystal growth velocities in pure metals and simple alloys. We are currently searching for system with a large enough difference in reflectivity between the crystalline and liquid phases, so that the pump-probe technique, developed for the silicon work, can be applied.

We have designed and finished the construction of a dual gun ion beam

sputtering system for preparing starting alloys for irradiation. It has produced very satisfactory pure metal films; we expect to produce the first compositionally modulated materials in the next month.

List of Papers

1. 'Solidification morphology of picosecond pulsed laser quenched $Fe_{96}B_4$', C.-J. Lin and F. Spaepen, Scripta Met., 17, 1259 (1983).

2. 'Picosecond pulsed laser-induced melting and glass formation in metals', C.-J. Lin, F. Spaepen and D. Turnbull, 5th Int. Conf. on Liquid and Amorphous Metals, to appear in J. Non-Cryst. Solids.

3. 'Metallic glasses and metastable crystalline phases produced by picosecond pulsed laser quenching', C.-J. Lin and F. Spaepen, Mat. Res. Soc. Conf. Symposia, in press.

These papers are added in appendix; two earlier papers, supported by the Harvard MRL, have been added for completeness of the alloy survey.

Thesis Completed:

C.-J. Lin, 'Formation of metallic glasses by picosecond pulsed laser quenching', 1983.

Time-resolved temperature measurement of picosecond laser irradiated silicon

L. A. Lompré,[a] J. M. Liu,[b] H. Kurz, and N. Bloembergen
Gordon McKay Laboratory, Division of Applied Sciences, Harvard University, Cambridge, Massachusetts 02138

(Received 22 March 1983; accepted for publication 26 April 1983)

Time-resolved reflectivity and transmission measurements of crystalline silicon films reveal lattice heating through the temperature dependence of the complex index of refraction. The temperature rise, which is much higher than derived by others from Raman scattering experiments, occurs in a surface layer of 100-nm thickness.

PACS numbers: 79.20.Ds

While the recent results[1-5] on the fundamental mechanisms of pulsed laser anealing of silicon are consistent with a simple thermal model, Raman scattering experiments[6,7] still suggest that the phase transition occurs far below the melting point, and that the lattice temperature remains below 800 K. It is the purpose of this letter to report a temperature determination form the variation in the complex index of refraction following a pump pulse.

Our earlier experiments utilized a probe pulse at $\lambda = 1064$ nm, following a pump pulse at $\lambda = 532$ nm. These data revealed the existence of a dense electron-hole plasma[8,9] with a lifetime of about 100 ps. A sharp transition to a molten metallic phase occurred at a pump fluence of 0.2 J/cm^2. Here, we report data on the reflectivity and transmission of thin samples of silicon-on-sapphire (SOS), at a probe wave-

[a] Permanent address: C. E. N./Saclay, DPh.G/S.P.A.S., 91191 Gifsur-Yvette Cedex, France.

[b] Permanent address: Department of Electrical and Computer Engineering, Bell Hall, SUNY at Buffalo, Amherst, New York 14260.

 0003-6951/83/140168-03$01.00

length $\lambda = 532$ nm and with a delay of 200 ps after the pump pulse. Under these conditions the plasma contribution to the index variations is minimized.[9] The latter can now be interpreted by their known intrinsic temperature variation, owing to the change in the indirect band gap and in the matrix elements for the indirect transition. While in the Raman scattering only the LO-branch phonons near the center of the Brillouin zone are involved, the index variations are determined by the thermal excitations of all phonon branches.[10] According to Jellison and Modine[11] the real part of the index in the green varies as $n = n_0 + \beta T$, with $n_0 = 3.93$ and $\beta = 6 \times 10^{-4}$ up to $T = 1000$ K. The imaginary part varies as $k = k_0 \exp(T/\Theta)$, with $k_0 = 4.24 \times 10^{-2}$ and $\Theta = 430$ K.

The experimental setup is similar to that described in Ref. 9. Simultaneous reflectivity and transmission measurements were performed on silicon-on-sapphire (SOS) samples with (100) silicon surfaces and with silicon films of 0.5- or 0.1-μm thickness. The SOS sample is heated by a pulse of 20 ps at 532 nm. The probe pulse is derived from the pump pulse with a beamsplitter. The variable time delay of the probe pulse with respect to the pump pulse can be extended from -50 ps to 2.5 ns. Zero time delay was determined with an accuracy of ± 5 ps. The polarization of the probe beam is rotated by 90° in a half-wave plate to suppress interference of the two beams on the sample surface. The probe beam is incident at 26° to the normal of the sample surface. The pump beam is incident on the opposite side of the normal and travels in a direction opposite to the probe beam. Because the pump and probe pulses are at the same wavelength, these precautions are necessary to prevent artifacts generated by the interference of pump and probe. Narrow band filters are used in front of the photodiode detectors to eliminate stray light at other wavelengths. The noise level of the detection system under regular experimental conditions is checked by blocking only the probe beam. The detection limit for transmission measurements is one percent. The pump pulse is focused to a diameter of 300 μm at the e^{-1} intensity contour of its Gaussian spatial profile. The probe pulse is focused to a diameter of 30 μm at the exact center of the pump spot. Because silicon has considerable absorption at 532 nm, which increases significantly with heating, the fluence of the probe pulse must be kept extremely low to prevent reheating or assisting the heating of the sample. In this experiment the probe fluence was kept at about 0.1% of the pump fluence.

At $\lambda = 532$ nm, the (100) silicon film of 0.5-μm nominal thickness exhibits sensitive changes of low intensity reflectivity and transmission owing to slight variations of the thickness across the sample. Without pumping, the reflectivity R and transmission T of the film at the probe incident angle of 26° change across the sample from a maximum value of $R = 0.52$ and a minimal value of $T = 0.27$ to a minimal value of $R = 0.15$ and a maximal value of $T = 0.48$. These interference effects, owing to reflection from the silicon-sapphire interface, provide an additional check on our experimental procedure. The derived values of $n + ik$ should be independent of the film thickness. This was indeed found to be the case. Film thicknesses which give the highest transmission at room temperature yield the most sensitive information on the variation of k with temperature.

In Fig. 1 the reflectivity and transmission of a 0.5-μm-thick SOS sample are plotted versus incident fluence F of the heating pulse after a time delay of 200 ps. With an increasing fluence level the reflectivity increases gradually and reaches a plateau between 0.12 and 0.16 J/cm^2. Above this level a sharp rise to a level of 69% occurs, which corresponds to the metallic reflectivity of liquid silicon at the angle of incidence used in this experiment. The flat top portion reflects the condition where multiple interferences are nearly suppressed because of the high absorption at elevated temperatures.

The transmission drops continuously from an initial value of 48% to the detection limit of 1% at 0.2 J/cm^2. This limit corresponds to an average optical absorption $\alpha > 7 \times 10^{+4}$ cm^{-1}, nearly one order of magnitude above the room-temperature value of $\alpha \sim 10^4$ cm^{-1}. The optically in-

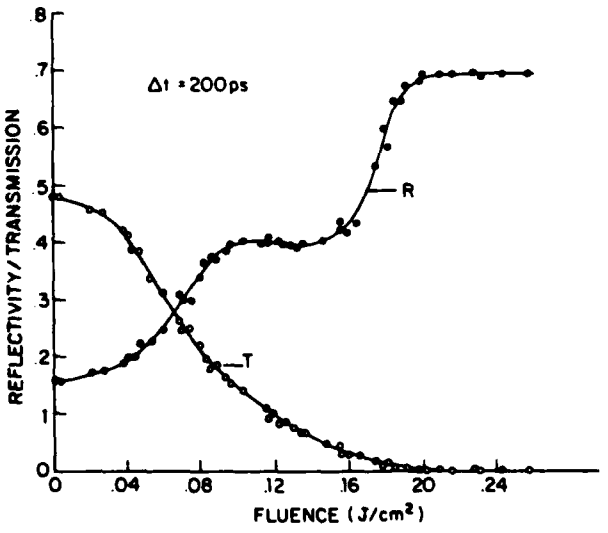

FIG. 1. Reflectivity and transmission at $\lambda = 532$ nm, probed with a delay $\Delta t = 200$ ps after the pump pulse at $\lambda = 532$ nm, vs incident fluence, in a 0.5-μm-thick SOS sample.

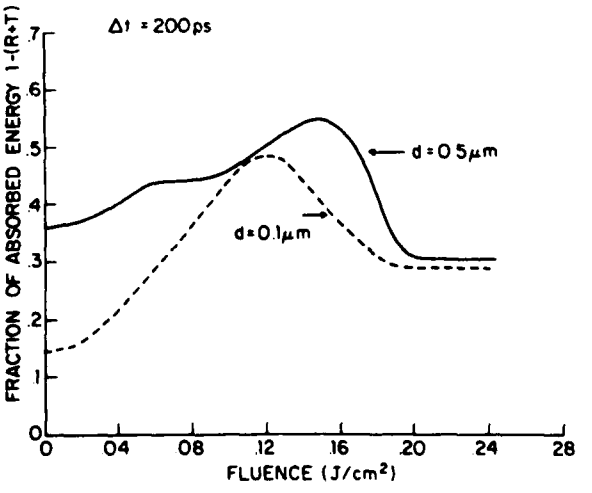

FIG. 2. Fraction of absorbed probe pulse energy vs incident energy fluence of the pump beam for the case of (a) a 0.5-μm-thick and (b) a 0.1-μm-thick SOS sample.

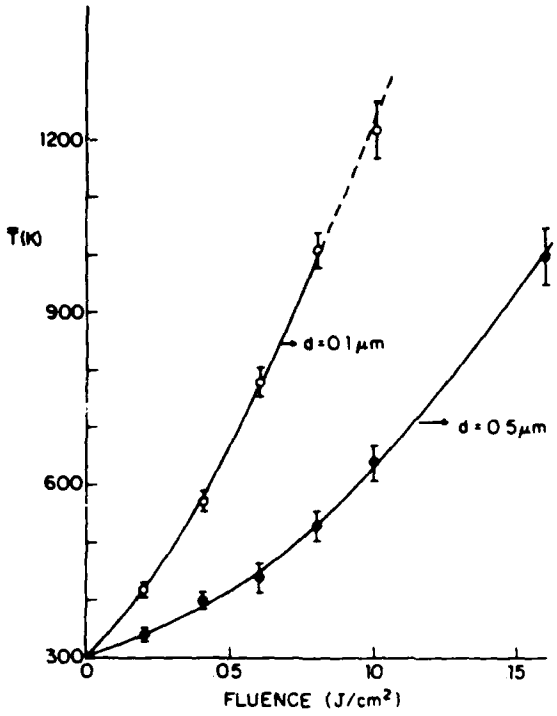

FIG. 3. Average temperature rise $\bar{T}$ in the two samples vs incident pump energy fluence.

duced transmission and reflectivity changes remain constant between 200 ps and 1 ns, indicating two facts: a local equilibrium between phonons is established in less than 200 ps, and no significant heat loss into the substrate occurs on a 1-ns time scale.

Direct experimental evidence for a large gradient of the absorption profile $\alpha(x)$ generated after 200 ps can be deduced from the absorbance of samples with different thickness. As shown in Fig. 2, the fraction of absorbed energy $A = [1 - (R + T)]$ of the probing pulse depends on the incident fluence F. At low fluence the quantity A is remarkably different for the 0.5 and 0.1-μm-thick silicon films. With increasing fluence the difference in A between the two samples is reduced. At a pump fluence level of 0.12 J/cm^2, even the thin sample absorbs most of the transmitted probe radiation. The slight modulation of the absorbance is caused by changing the standing wave pattern of the pump beam during the irradiation.

The actual temperature profile $T(x)$ is crucial for fitting the measured reflectivity and transmission data. Due to the exponential temperature dependence of α, the optical density

$$\alpha d = \int_0^d \alpha(x)dx = \alpha_0 \int_0^d \exp\left(\frac{T(x)}{\theta}\right)dx$$

depends critically on the profile $T(x)$. According to the thin-film optics equations for continuously varying refractive index, the correlation between reflectivity and transmission requires a precise knowledge of the spatial profile of the optical thickness.[12] We have not been able to match the transmission and reflectivity data, assuming a uniform temperature distribution even in the thin SOS sample ($d = 1000$ Å). If temperature profiles are calculated numerically from the nonlinear absorptivity $\alpha(T)$, the observed reflectivity and transmission data can be matched through the entire range of fluences below the threshold for phase transition. A detailed analysis of this fitting procedure is beyond the scope of this letter and will be published in an extended version. Here, only the resulting average value of the temperature,

$$\bar{T} = d^{-1} \int_0^d T(x)dx,$$

is shown in Fig. 3 to indicate the actual heating of the lattice. $\bar{T}$ is a nonlinear function of the energy fluence as the absorptivity changes during the 20-ps heating pulse. In the thin sample with $d = 100$ nm, an average temperature rise of 1000 K occurs at a pump fluence of 0.08 J/cm^2. Since the data in Ref. 11 only go to 1000 K, the behavior at higher temperatures cannot be plotted. The actual surface temperature is, of course, still higher.

These optical probing experiments reveal significantly higher lattice temperatures than have been inferred from Stokes–anti-Stokes ratios in Raman scattering experiments. Our signal to noise is, of course, many orders of magnitude better than in the Raman case. In fact, the temperature rise can be determined for a single individual pulse. When our temperature data are extrapolated to higher fluences, they are consistent with the attainment of the melting point at the observed fluence threshold of 0.2 J/cm^2 for a phase transition, prevously reported.[9]

[1] C. W. White and P. S. Pearry, eds., *Laser and Electron Beam Processing of Materials* (Academic, New York, 1980).
[2] J. F. Gibbons, L. D. Hess, and T. W. Sigmon, eds., *Laser and Electron Beam Solid Interactions and Material Processing* (North-Holland, Amsterdam, 1981).
[3] B. R. Appleton and G. K. Celler, eds., *Laser and Electron Beam Interactions with Solids* (North-Holland, Amsterdam, 1982).
[4] J. M. Liu, R. Yen, H. Kurz, and N. Bloembergen, in *Laser and Electron Beam Interactions*, edited by B. R. Appleton and G. K. Celler (North-Holland, Amsterdam, 1982), p. 29.
[5] S. Stritzker, B. Pospieszczyk, and J. A. Tagle, Phys. Rev. Lett. 47, 356 (1981).
[6] A. Campaan, M. W. Loo, A. Aydinli, and M. C. Lee, in *Laser Solid State Interactions and Transient Thermal Processing*, edited by J. Narayan, N. L. Brown, and R. A. Lemmons (Elsevier, New York, 1983).
[7] D. von der Linde, G. Hartmann, and A. Ozols, in *Laser Solid State Interactions and Transient Thermal Processing*, edited by J. Narayan, N. L. Brown, and R. A. Lemnins (Elsivier, New York, 1983).
[8] J. M. Liu, thesis, Harvard University, 1982.
[9] J. M. Liu, H. Kurz, and N. Bloembergen, Appl. Phys. Lett. 41, 643 (1982).
[10] R. A. Smith, *Semiconductors*, 2nd ed. (Cambridge University, Cambridge, England, 1978), p. 321.
[11] G. E. Jellison, Jr. and F. A. Modine, Appl. Phys. Lett. 41, 180 (1982), and private communication.
[12] R. Jacobsson, in *Progress in Optics*, edited by E. Wolf (North-Holland, Amsterdam, 1966), Vol. V, p. 249.

Accepted for publ. in Appl. Phys. Lett

Optical heating of electron-hole plasma in silicon by picosecond pulses

L.-A. Lompré, J.-M. Liu, H. Kurz and N. Bloembergen

Gordon McKay Laboratory, Division of Applied Sciences, Harvard University, Cambridge, Massachusetts 02138

(Received

Using a novel three-pulse technique, essential information about the density, optical effective mass and kinetics of laser-generated plasmas in silicon has been obtained.

PACS numbers: 52.50
72.30
79.20Ds

Numerous investigations of the change in optical properties of silicon induced by a strong pump or 'heating' pulse have recently been carried out [1-4]. By varying the wavelength of the probing pulse and its time delay with respect to the picosecond pump pulse, the contributions due to a variation in lattice temperature and those due to changes in carrier density have been separately determined [5].

The real part of the dielectric function at a probing frequency ω:

$$\varepsilon' = n_L^2(T)[1 - \kappa^2(T)] - \frac{4\pi e^2 N}{m^* \omega^2} \qquad (1)$$

increases with the lattice temperature T ($dn/dT > 0$, $\kappa^2 < 1$) and decreases with the number of electron-hole pairs N. As long as there is no reliable information about the modification of the optical reduced mass $m^* = (m^{*-1}_e + m^{*-1}_h)^{-1}$ at high densities and carrier temperatures T_e available, the reflectivity data of laser-generated plasmas in silicon allow only the determination of N/m^*.

The imaginary part of the dielectric function

$$\varepsilon'' = 2n_L^2(T)\,\kappa_L(T) + \frac{4\pi e^2 N}{\omega^3}\left(\frac{1}{m^*_e\langle\tau_e\rangle} + \frac{1}{m^*_h\langle\tau_h\rangle}\right) \qquad (2)$$

increases with N and T; however, as a third unknown parameter, the scattering times of the carriers (τ_e,τ_h) averaged over their energy distribution come into play. Thus the experimental determination of ε' and ε'' do not provide sufficient information to solve separately for N_e, T_e and m^*.

In this note results obtained with a three-pulse technique are

reported. The first pulse, with a fluence of 50 mJ/cm^2 in the visible (λ = 530 nm) of 20 ps duration, creates the carrier plasma. A second pulse at λ = 1.06 μm of 30 ps duration adds energy to the plasma by the free carrier absorption processes without changing its density. A third pulse (λ = 530 nm) probes the resulting changes in reflectivity and transmission of a 0.5 μm thick silicon-on-sapphire (SOS) sample. Details of the experimental geometry have been given in reference 5.

The time delay between the first two pulses is kept fixed, Δt_{21} = 100 ps. Then the reflectivity and transmission as a function of Δt_{31}, the time delay of the probe pulse, is shown in Fig. 1 for two cases. The drawn lines are valid in the absence of the second pulse. This behavior has been explained previously [5] in terms of decaying plasma density and with the asymptotic values of R and T indicating the change in lattice temperature. The dotted lines are valid when the IR plasma heating pulse of 25 mJ/cm^2 is applied. The data give the variations ΔR and ΔT, due to the change in lattice temperature. There is no evidence for an increase in N/m^* due to the second pulse. The data indicate that the energy relaxation time τ_W of the carriers with the lattice is faster than impact ionization.

In Fig. 2 the probe pulse is fixed at Δt_{31} = 400 ps. The change in reflectivity ΔR is measured as a function of Δt_{21}. It therefore measures the variation in the lattice temperature ΔT. Clearly, the additional heating by the second pulse of 40 mJ/cm^2 is maximum for Δt_{21} = 10 ps and decays as the plasma density created by

the first pulse decays.

These data are consistent with a model in which the energy relaxation time τ_W between carriers and lattice is taken to be short compared to the pulse duration. In fact, we have put $\tau_W = 0$. Instantaneous thermal enhancement of the indirect absorption at 0.53 μm is assumed. Thus the generation rate of electron-hole pairs experiences a significant increase [6] during the picosecond excitation at 0.53 μm. With these assumptions, the highest possible plasma densities in the absence of impact ionization are calculated. The results for a fluence level of $F_0^{2\omega} = 100$ mJ/cm^2 are shown in Fig. 3, where the plasma density at the surface N_s and the surface temperature T_s are plotted versus time. The plasma density reaches the maximum with $\sim 6.7 \times 10^{+20}$ cm^{-3} a few picoseconds after the intensity maximum of the Gaussian temporal excitation profile centered at $\Delta t = 0$. The plasma density is strongly reduced by Auger recombination ($\gamma = 4 \times 10^{-31}$). The rise and peak of the lattice temperature are retarded with respect to the plasma features.

Optical probing of the plasma generated at this fluence level yields an upper limit of N/m^* values with $N/m^* = 4 \times 10^{48}$ g^{-1} cm^{-3} [3,4,7]. The maximum possible value of the optical mass at this fluence level is $m^* \leq 0.18\ m_0$. Thus the data are consistent with a nearly constant reduced optical mass $m^* = (m_e^{-1} + m_h^{-1})^{-1} = 0.15\ m_0$, expected for a plasma in thermal equilibrium with the lattice.

The solid lines in Fig. 2 are calculated on the basis of this model with the free carrier absorption cross section at 1.06 μm taken to be $\sigma = 2.3 \times 10^{-17}$ (T/300). This coefficient is four times

times larger than that reported at lower carrier concentrations [8]. The carrier momentum relaxation times τ_e and τ_h, occurring in Eq. (2), are drastically reduced at high t -peratures and high plasma densities; or, alternatively, the Drude model does not adequately describe the absorption. A more complete theoretical discussion will be presented elsewhere.

In conclusion, the three-pulse experiments support the picture that the carrier plasma rapidly cools off by transferring energy to the lattice. Plasma heating by free carrier absorption does not lead to significant impact ionization. The 'simple heating' model equations yield the correct plasma density and temperature on a picosecond time scale. The real part of the dielectric constant is consistent with a low value of the effective mass, and the imaginary part indicates a shortening of the momentum relaxation times.

This work was supported by the U.S. Office of Naval Research under contract no. 00014-83K-0030. One of us (H.K.) would like to acknowledge partial support from the Alexander von Humboldt Foundation, Bonn, R. R. Germany.

REFERENCES

1. D. H. Auston, C. M. Surko, T. N. C. Venkatesan, R. E. Slusher, and J. A. Golovchenko, Appl. Phys. Lett. 33, 437 (1978).

2. J. M. Liu, R. Yen, H. Kurz, and N. Bloembergen, Appl. Phys. Lett. 39, 755 (1981). R. Yen, J. M. Liu, H. Kurz, and N. Bloembergen, Appl. Phys. A 27, 153 (1982).

3. J. M. Liu, H. Kurz, and N. Bloembergen, Appl. Phys. Lett. 41, 643 (1982).

4. D. von der Linde, and N. Fabricius, Appl. Phys. Lett. 41, 991 (1982).

5. L. A. Lompré, J. M. Liu, H. Kurz, and N. Bloembergen, Appl. Phys. Lett. 43, 168 (1983).

6. A. Lietoila and F. Gibbons, Appl. Phys. Lett. 40, 624 (1982).

7. H. van Driel, L. A. Lompré, and N. Bloembergen, to be published in Appl. Phys. Lett.

8. K. G. Svantesson, J. Phys. D: Appl. Phys. 12, 425 (1979).

FIGURE CAPTIONS

1. Time-resolved reflectivity and transmission in SOS induced by the first pump pulse at 532 nm with 50 mJ/cm^2 and probed at the same wavelengths at different time delays (full line). Changes induced by the second pump beam at 1064 nm with 25 mJ/cm^2 (dotted line).

2. Relative changes of reflectivity and transmission probed after 400 ps, induced by a second pulse at 1064 nm with a fluence F_0^{ω} = 40 mJ/cm^2. The ΔR and ΔT values are measured as a function of its delay time Δt_{21}.

3. Calculated temporal profile of the plasma density $N = N_e = N_h$ and lattice temperature at the surface of silicon during and following a 20ps, 0.1 J/cm^2 pump pulse at 0.53 μm.

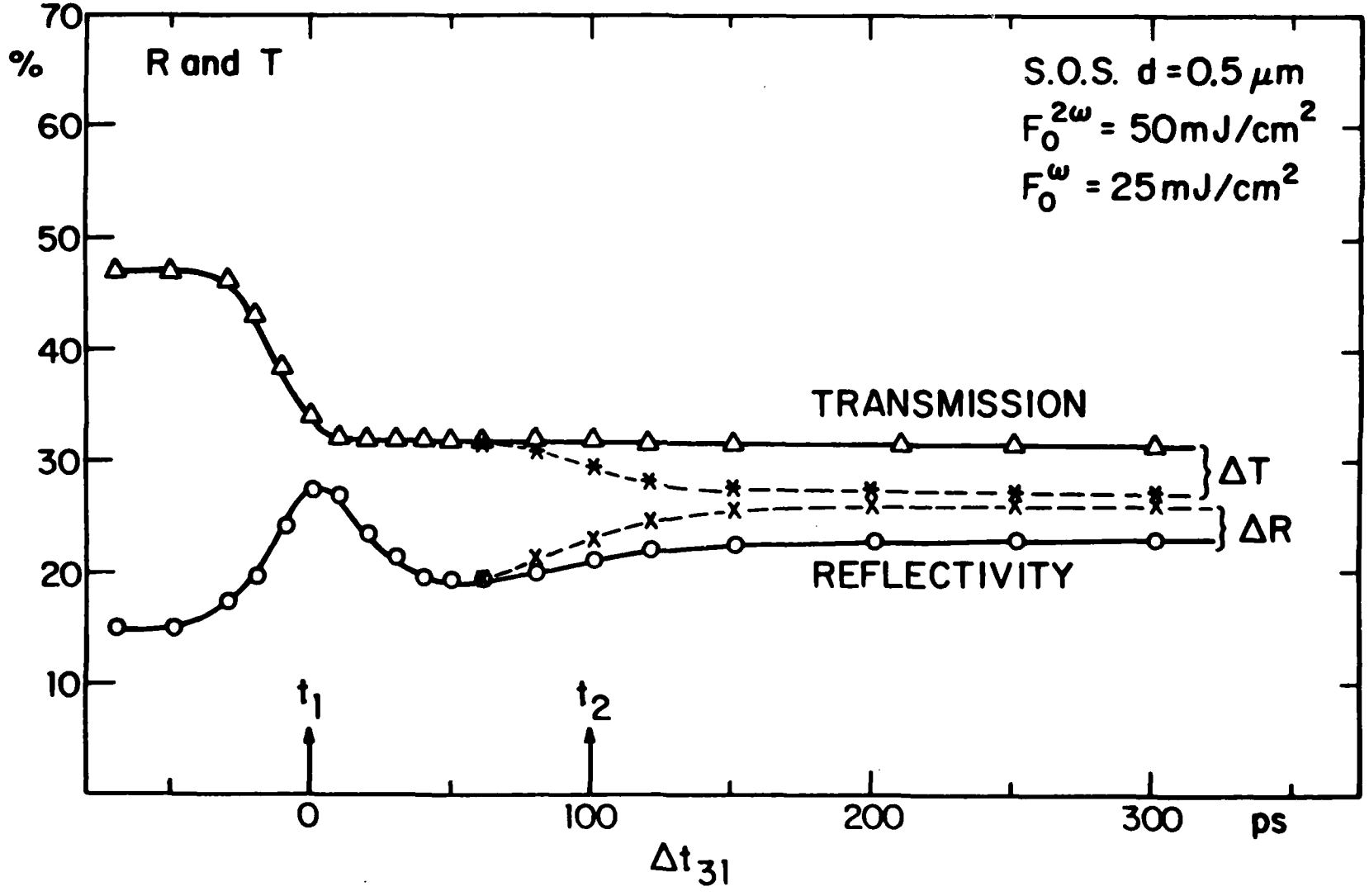
70
%
R and T
S.O.S. d = 0.5 μm
$F_0^{2\omega}$ = 50mJ/cm²
F_0^{ω} = 25mJ/cm²
60
50
40
TRANSMISSION
30
ΔT
ΔR
20
REFLECTIVITY
10
t_1
t_2
0
100
200
300
ps
Δt_{31}

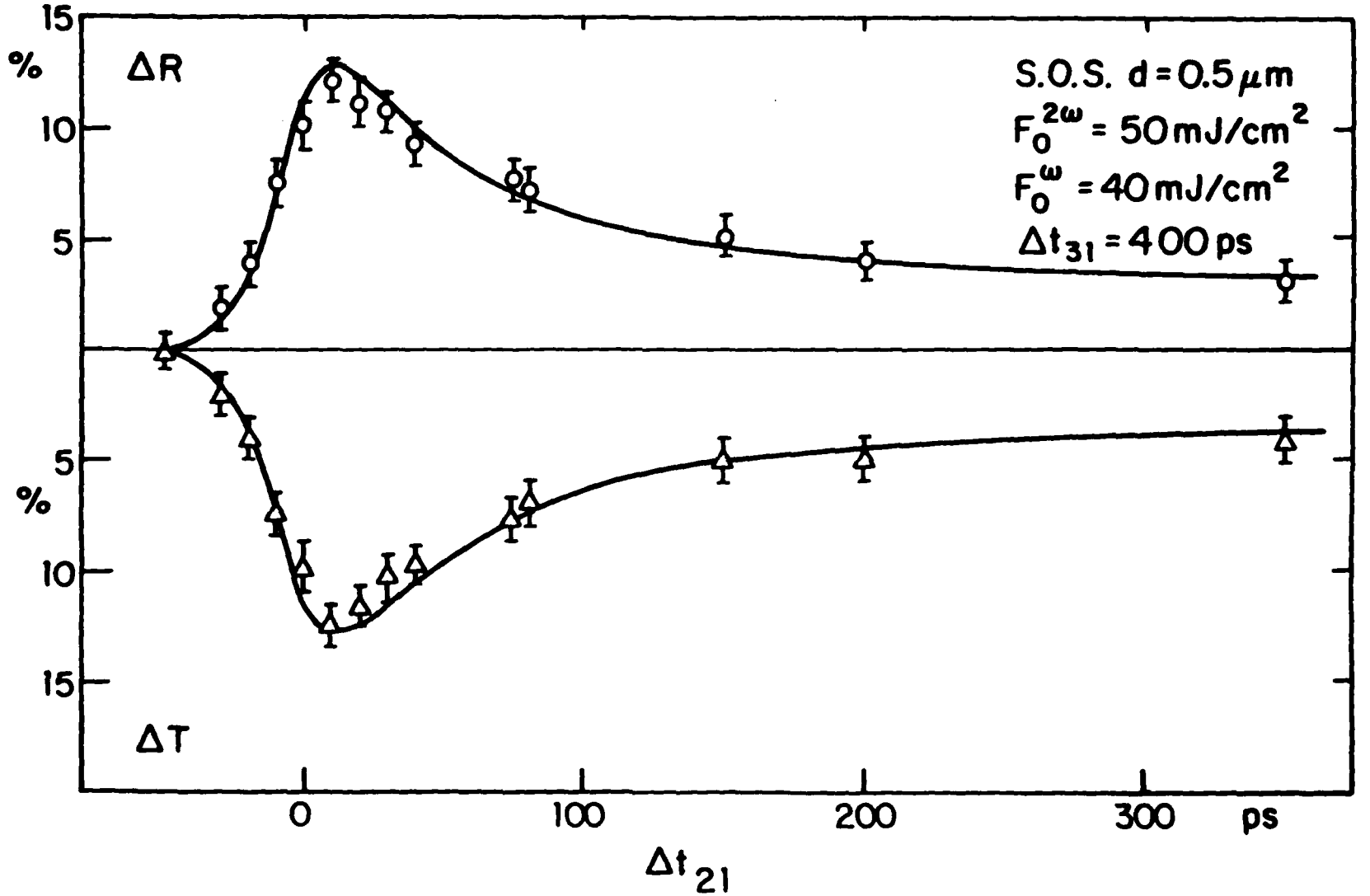
15
%
ΔR
10
5
S.O.S. d = 0.5 μm
$F_0^{2\omega}$ = 50 mJ/cm²
F_0^{ω} = 40 mJ/cm²
Δt_{31} = 400 ps
5
%
10
15
ΔT
0
100
200
300
ps
Δt_{21}

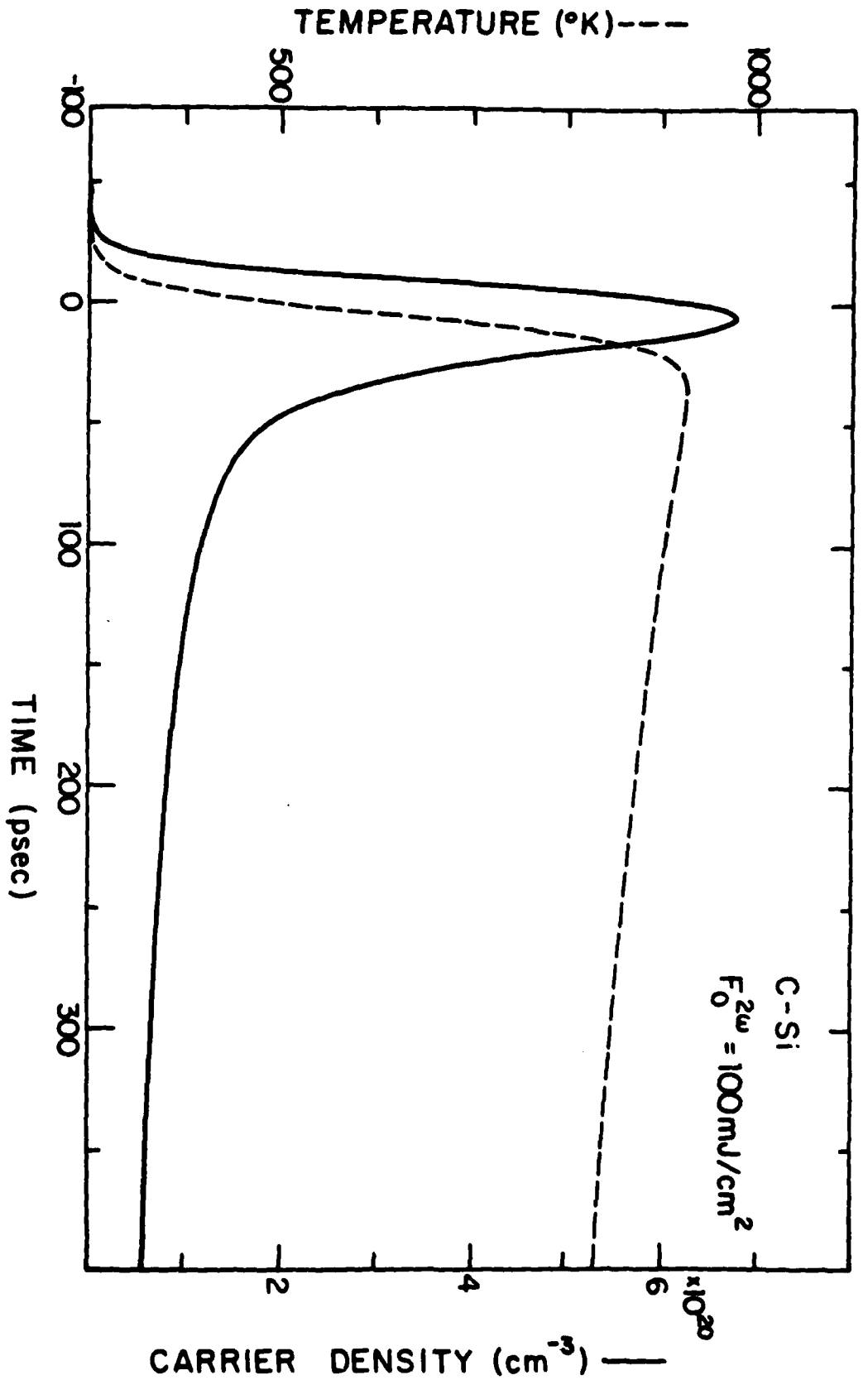
TEMPERATURE (°K)---
500
1000
-100
0
100
200
300
TIME (psec)
C-Si
$F_0^{2\omega}$ = 100mJ/cm^2
2
4
6
×10^{20}
CARRIER DENSITY (cm^{-3}) ——

Accepted for Publ.
in Appl. Phys Letters

Picosecond time-resolved reflectivity and transmission at 1.9 and 2.8 μm of laser-generated plasmas in silicon and germanium

H.M. van Driel,[a] L.-A. Lompré,[b] and N. Bloembergen

Gordon McKay Laboratory, Division of Applied Sciences, Harvard University, Cambridge, Massachusetts 02138.

(Received

We have observed plasmon resonances with 1.9 μm and 2.8 μm probe pulses in silicon and germanium, excited by 25 ps pulses up to 40 mJ/cm^2 at 0.53 and 1.06 μm, respectively. Firm values of N/m^* are derived.

The kinetics of laser generated electron-hole plasmas in semiconductors and their possible influence on phase transitions have been of considerable interest, particularly in the area of laser annealing of ion-implanted materials.[1] One of the most direct techniques which can be used to obtain the carrier density and its temporal and spatial evolution involves time resolved free carrier infrared spectroscopy[2] with the ambipolar plasmas probed in reflection and/or transmission. This technique has been used[3,4] in nonosecond and picosecond time scales to observe transient plasmon resonances at 5.4 and 10.6 μm in Ge, Si and GaAs for plasma densities of 10^{19} to 10^{20} cm^{-3}. To investigate higher densities in Si, several researchers have used high picosecond or femtosecond excitations with probe pulses at wavelengths ≤ 1.06 μm.[5] Although a free carrier induced drop in the reflectivity is observed in all cases, the enhanced reflectivity associated with the plasmon resonance is not. Due to a lack of knowledge of the detailed dielectric function at high excitation levels, it is difficult to extract quantitative information about the plasma parameters from such experiments. However, even assuming the validity of Drude-Zener formalism, optical measurements allow only the evaluation of N/m^*, where N is the plasma density and m^* the electron-hole reduced conductivity effective mass.[6] From previous experiments employing a 1.06 μm picosecond probe a normalized density of $N/m^* = 3.4 \times 10^{48}$ $g^{-1}cm^{-3}$ has been found for a 0.53 μm, 25 ps., 100 mJ/cm^2 excitation pulse.[6] According to the Drude model the plasmon resonance would therefore be expected at a wavelength of

$$\lambda = c/e(m^*/N_p)^{1/2}(\pi\varepsilon_\infty)^{1/2} \simeq 2\ \mu m \qquad (1)$$

where $\varepsilon_\infty = 11.8$ is the high frequency dielectric constant.

In this letter we report the direct observation of the plasmon resonances by using picosecond probe pulses at 1.9 and 2.8 μm. A firm value of N/m* is derived.

A passively mode-locked Nd:YAG laser was used to produce single 30 ps., 1.06 μm and 25 ps., 0.53 μm pulses which had Gaussian spatial and temporal profiles. These pulses were respectively focussed to spot sizes of 800 μm diameter (e^{-1} intensity points) on (111) surfaces of nearly intrinsic Ge and Si wafers. The back surface of these samples was optically diffuse and so prevented undesired interference effects. The generated plasmas were probed in reflection (R) and in transmission (T) using 1.9 and 2.8 μm pulses which were derived from a portion of the initial 1.06 μm pulse by the stimulated Raman scattering in 50 cm long cells containing 50 atmospheres of H_2 and CH_4, respectively. The first stokes component from the H_2 gas and the second stokes component from the CH_4 gas were selected using interference filters. The pulse widths, although not measured, are estimated[7] to be less than 30 ps.. The probe pulses, whose spatial profile was measured to be close to diffraction limited, were focused to spot sizes of $\leq$ 200 μm at the center of the excitation region; their fluence was kept less than 1 mJ/cm^2 to avoid undesired heating effects. Three PbS detectors were used to measure reflected, transmitted and reference probe pulse energies,while a calibrated vacuum photodiode was used to monitor pump energies. The signals from all four detectors were handled by a computer-automated data acquisition system. Standard picosecond pump and probe techniques were used to determine R and T as a function of time.

Figures 1-3 display typical results for the time resolved reflectivity and transmission signatures in silicon and germanium for different pump fluences. The curves accompanying the data are guides to the eyes. The pump

fluence was kept below the threshold fluence for melting (200 mJ/cm^2 in Si at 0.53 μm, 75 mJ/cm^2 in Ge at 1.06 μm) to avoid any contributions from metallic or molten regions. Complete theoretical interpretation of these results will be given elsewhere.[8] Here we wish to illustrate the salient features for different excitations and probe conditions. Figure 1 shows the reflectivity R at 1.9 μm as a function of time for Si for a 40 mJ/cm^2 pump fluence. At 40 mJ/cm^2, and below, the transient R shows a broad single minimum. Within the Drude-Zener model, the true minimum is reached when the real part of the dielectric constant is unity, which occurs at a critical density $N_c = (\varepsilon_\infty - 1/\varepsilon_\infty)N_p$, where N_p is given by equation (1). The value of the reflectivity at the minimum, R = 0.12, is determined by the plasma damping mechanism and the temporal width of the probe pulse. The non-zero width of the probe pulse unfortunately partially washes out the actual transient optical response of the plasmon resonance. However, at least for the broad minimum in R, at low fluences, these effects are small. Assuming that the convolution effects do not change the value of the minimum reflectivity, a value of $N/m^* = 3.6 \times 10^{48}\ g^{-1}cm^{-3}$ is derived. If one assumes for the effective mass, $m^* = 0.123\ m_o$, (the low density value) where m_o is the free electron mass, the plasma density would be $4 \times 10^{20}\ cm^{-3}$ at the pump fluence of 40 mJ/cm^2. Theoretical considerations[9] indicate that m*, and consequently N, may be up to factor two higher at this level of irradiation.

The transmission data, normalized to the bulk transmission of an unexcited sample, provides complementary information to that of the reflectivity, since it is sensitive to the total number of carriers in the bulk. The normalized transmission, T, is given by

$$T(t) = (0.7)^{-1}(1 - R(t)) \exp\left(-\sigma \int_0^\infty N(x)dx\right) \qquad (2)$$

where 0.7 is the surface transmission of the unexcited sample. This equation is justified if σ, the free carrier absorption cross-section, is independent of depth, x. The transmission drops to a minimum of 10% at 40 mJ/cm^2. This transmission minimum is located at a slightly positive time delay between the excitation and the probe pulses. This is a direct consequence of the temporal integration (nonzero probe pulse width). The free carrier induced transmission change recovered more slowly than the corresponding reflectivity trace, due to the fact that the plasma density at the surface is higher than the average density in the bulk.

Figure 2 shows typical experimental results obtained at 2.8 μm, where the plasmon resonance is easily observed. The 15 mJ/cm^2 data is similar to that of Fig. 1 and shows a broad single minimum. At 40 mJ/cm^2, the transient R shows two shallow minima on both sides of a peak near the zero time delay. During the leading and the trailing edge of the pump pulse, the carrier surface density passes twice through the critical density N_c. Deconvolution of the data with respect to the nonzero probe pulse width indicates that the peak reflectivity is > 0.9. The slower decay of R at 2.8 μm is as expected, since the reflectivity at the longer wavelength is more sensitive to a given density of carriers. The clear experimental observation of the plasmon resonance at 2.8 μm indicates that the N/m^* value passes twice through the value of 1.8×10^{48} $g^{-1}cm^{-3}$ on each side of the maximum value of 3.6×10^{48} $g^{-1}cm^{-3}$ at the same fluence of 40 mJ/cm^2. Apart from discrepancy near zero delay, where large fluctuations were noted, the transmission data at 40 mJ/cm^2 is consistent with equation (2) with $\sigma = 5 \times 10^{-17}$ cm^2.[10]

The data taken with the Ge sample is interesting, since it reveals apparent saturation of the carrier generation rate which has been the subject of speculations over the past few years.[11,12] Figure 3 shows R and T data

at 1.9 and 2.8 μm for Ge at 50 mJ/cm^2, 30% below the threshold for bulk melting. With a pump absorption depth of 0.7 μm, the carrier generation rate at 1.06 μm is higher than that of 100 mJ/cm^2 at 0.53 μm in Si. Also the Auger recombination coefficient[13] of 2×10^{-31} cm^6/sec is a factor of two smaller than in Si, as is the reduced effective mass. However, as shown, the plasmon resonance is not observed at 1.9 μm and is barely discernible at 2.8 μm. Theoretical considerations for germanium indicate that the reduced effective mass is not more than 20% greater than its low density value $m^* = 0.08\ m_o$. A detailed fit of the data shows that the maximum density obtained is $N = 2.5 \times 10^{20}$ cm^{-3}, while $N_p = 2.0 \times 10^{20}$ cm^{-3} for 2.8 μm. The observations at 2.8 μm are consistent with those at 1.9 μm where no reflectivity peak is observed, as this would require a density at the surface of 4.5×10^{20} cm^{-3}. The low densities are indicative of intravalence band absorption[12,14] or saturation of the valence-conduction band transition due to the Burstein-Moss effect. A model which neglects these processes would lead to a larger carrier density at the surface ($> 10^{21}$ cm^{-3}), which is not observed. The low minimum value of the transmission, shown here only for 1.9 μm, also indicates a stronger plasmon damping, due to the added contribution of intravalence band transitions. Lastly, it should be noted that the melting threshold of Ge at 1.06 μm is consistent with the absorption coefficient and the known melting temperature of 1210 K.

In summary, we have shown experimentally that the plasmon resonances are located between 1.9 and 2.8 μm for picosecond excitation pulses of 40 mJ/cm^2 on silicon and of 50 mJ/cm^2 on germanium. In silicon the maximum plasma density at the surface is 4×10^{20} cm^{-3} if variation of the effective mass is negligible, although both may be up to a factor of two higher. In

germanium the maximum carrier density is about 2 to 3×10^{20} cm^{-3} before melting occurs. These data show that fast infrared transient spectroscopy of Si and Ge is a valuable technique.

This research was supported by the Office of Naval Research under contract N00014-83-K-0030 and the Joint Services Electronics Program under contract N00014-75-C-00648.

REFERENCES

[a] Permanent address: Department of Physics and Erindale College, University of Toronto, Toronto, Canada, M5S 1A7.

[b] Permanent address: C.E.N./ Saclay, DPh.G./ S.P.A.S., 91191 Gif-sur-Yvette Cedex, France.

[1] See, for example, articles in: Laser and Electron Beam Interactions with Solids, ed. by B.R. Appleton and G.K. Celler (North Holland, Amsterdam, 1982); Laser-Solid Interactions and Transient Thermal Processing of Materials, ed. by J. Narayan, W.L. Brown, and R.A. Lemons (North Holland, Amsterdam, 1983).

[2] W.G. Spitzer and H.Y. Fan, Phys. Rev. 106, 882 (1957).

[3] G.N. Galkin, L.M. Blinov, V.S. Vavilov, and A.G. Solomatin, Pisma Zh. Eksp. Teor. Fiz. 7, 93 (1968)(JETP Letters 7, 69 (1968)); S.A. Jamison, A.V. Nurmikko, and H.J. Gerritsen, Appl. Phys. Lett. 29, 640 (1976); A.J. Alcock, P.B. Corkum, and P.J. James, Can. J. Phys. 57, 1280 (1979).

[4] P.C. Hein, M.I. Gallant, and H.M. van Driel, Solid State Commun. 39, 601 (1981); M.I. Gallant and H.M. van Driel, Phys. Rev. B 26, 2133 (1982); and J.S. Preston and H.M. van Driel, Phys. Rev. B (in press).

[5] J.M. Liu, H. Kurz, and N. Bloembergen, Appl. Phys. Lett. 41, 643 (1983); D. von der Linde and N. Fabricius, Appl. Phys. Lett. 41, 991 (1983); and C.V. Shank, R. Yen, and C. Hirliman, Phys. Rev. Lett. 50, 454 (1983).

[6] H. Kurz, L.-A. Lompré, and J.M. Liu, in Proc. of MRS-Europe Meeting, Strasbourg, 1983 (to be published in J. de Physique (Paris))

[7] R.L. Carman, M.E. Mack, F. Shimizu, and N. Bloembergen, Phys. Rev. Lett. 23, 1327 (1969); R.L. Carman, F. Shimizu, C.S. Wang, and N. Bloembergen, Phys. Rev. A 2, 60 (1970).

[8] H.M. van Driel, L.-A. Lompré, and N. Bloembergen (unpublished).

[9] H.M. van Driel (to be published in Appl. Phys. Lett.); see also M. Miyao, T. Matsuoka, N. Tatsuaki, and T. Tokuyama, Solid State Commun. 37 605 (1981).

[10] M. Balkanski, A. Aziza, and E. Amzallaq, Phys. Stat. Sol. 31, 323 (1969).

[11] A. Elci, M.O. Scully, A.L. Smirl, and J.C. Matter, Phys. Rev. B 16, 191 (1977).

[12] C.Y. Leung and M.O. Scully, Phys. Rev. B 23, 6797 (1981); A.L. Smirl, A. Miller, G.P. Perryman, and T.J. Boggess, J. de Physique (Paris) C 7, 463 (1981).

[13] D.H. Auston, C.V. Shank, and P. Lefur, Phys. Rev. Lett. 35, 1022 (1975).

[14] R.B. James, I.E.E.E. J. Quant. Elec. QE-19, 709 (1983).

FIGURE 1. Reflectivity and transmission of bulk Si at 1.9 μm as a function of probe time delay after a 0.53 μm pump pulse at 0.04 J/cm^2.

FIGURE 2. Reflectivity and transmission of bulk Si at 2.8 μm as a function of probe time delay after a 0.53 μm pump pulsed at (a) 0.015 J/cm^2 and (b) 0.04 J/cm^2.

FIGURE 3. Reflectivity and transmission of bulk Ge at 1.9 μm and 2.8 μm as a function of probe time delay after a 1.06 μm pulse of fluence 50 mJ/cm^2.

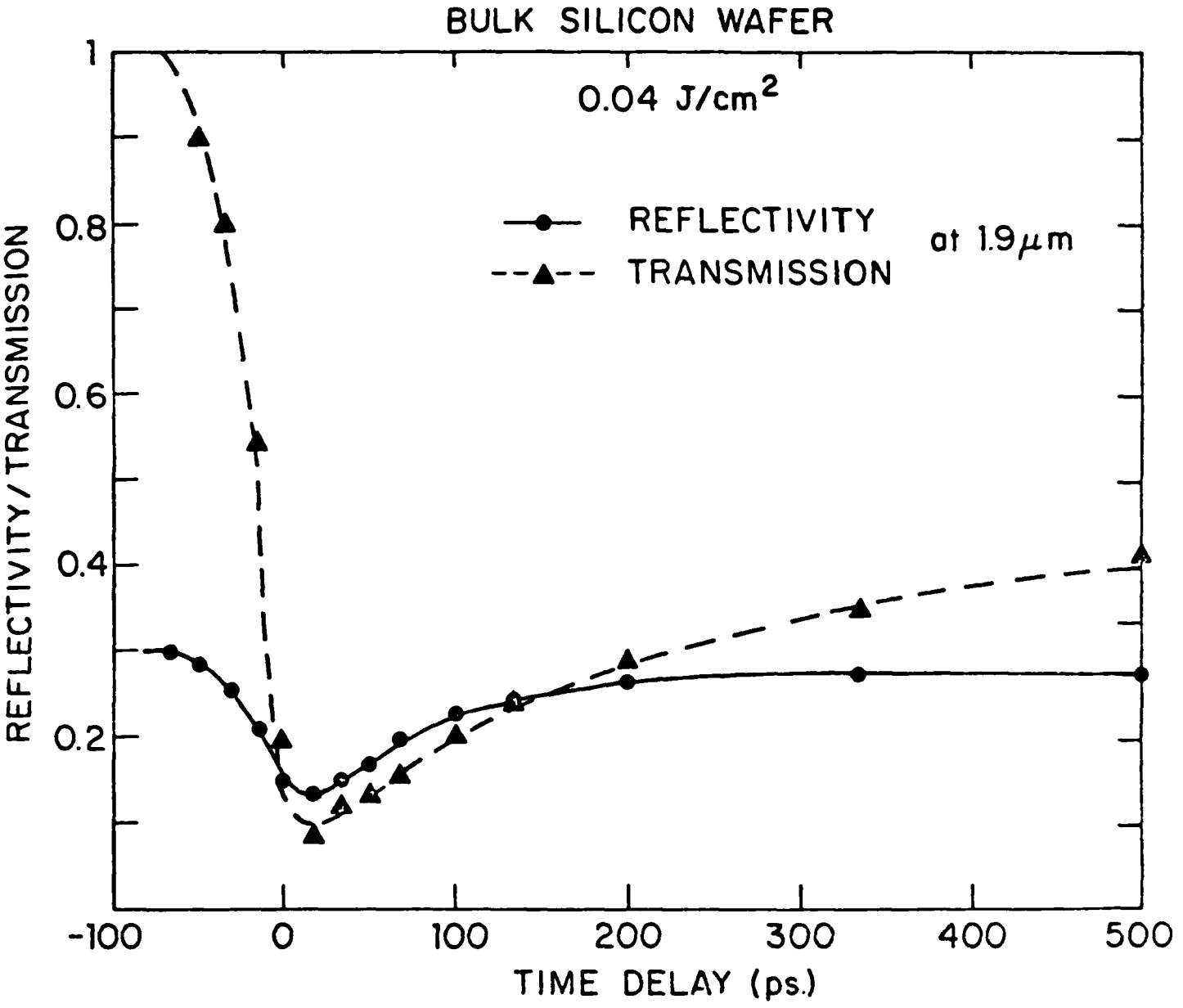
BULK SILICON WAFER
0.04 J/cm²
REFLECTIVITY
TRANSMISSION
at 1.9μm
REFLECTIVITY/TRANSMISSION
1
0.8
0.6
0.4
0.2
-100
0
100
200
300
400
500
TIME DELAY (ps.)

Figure 1

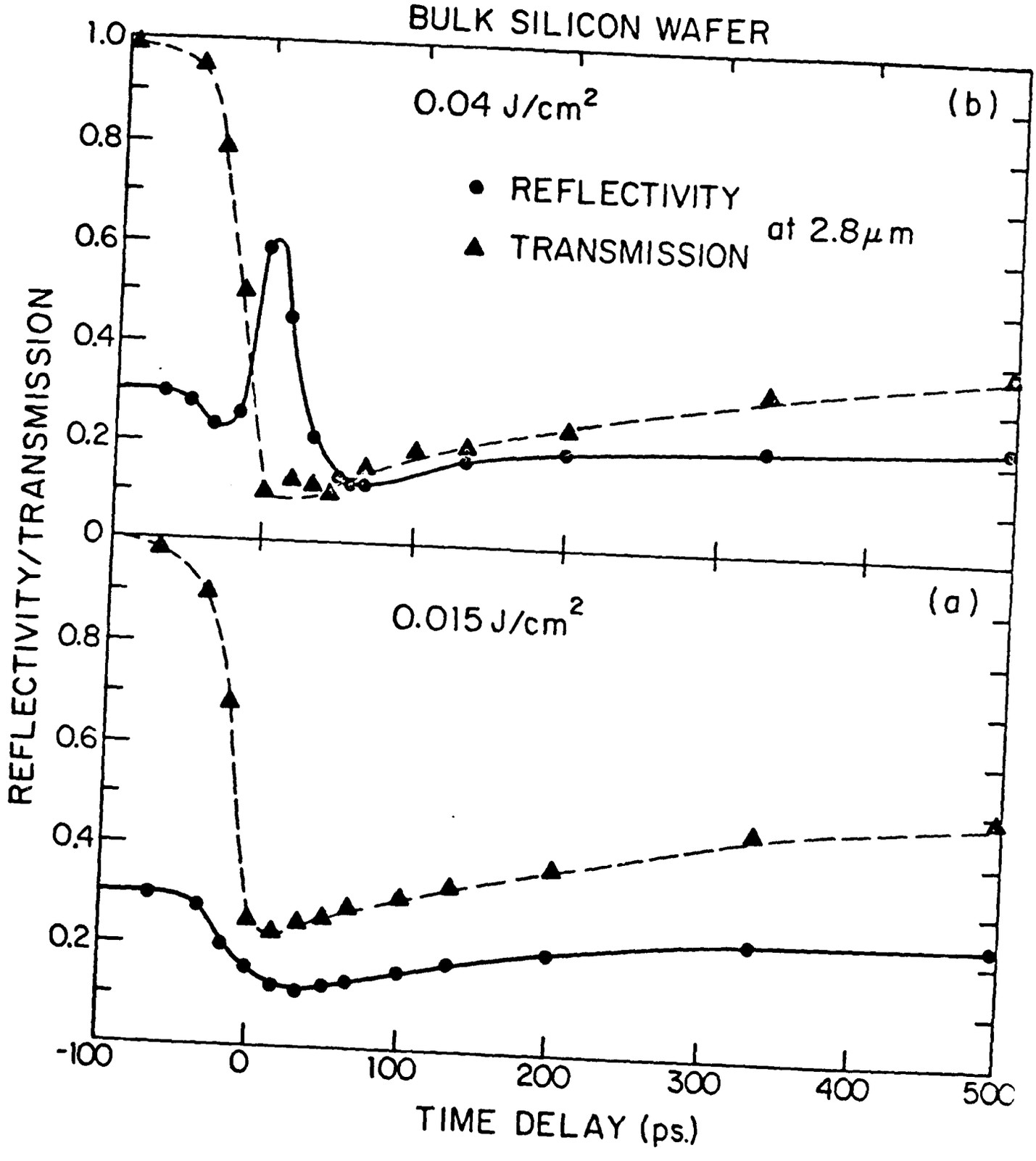
BULK SILICON WAFER
0.04 J/cm²
(b)
REFLECTIVITY
TRANSMISSION
at 2.8μm
0.015 J/cm²
(a)
REFLECTIVITY/TRANSMISSION
TIME DELAY (ps.)
1.0
0.8
0.6
0.4
0.2
0
-100
100
200
300
400
500

Figure 2

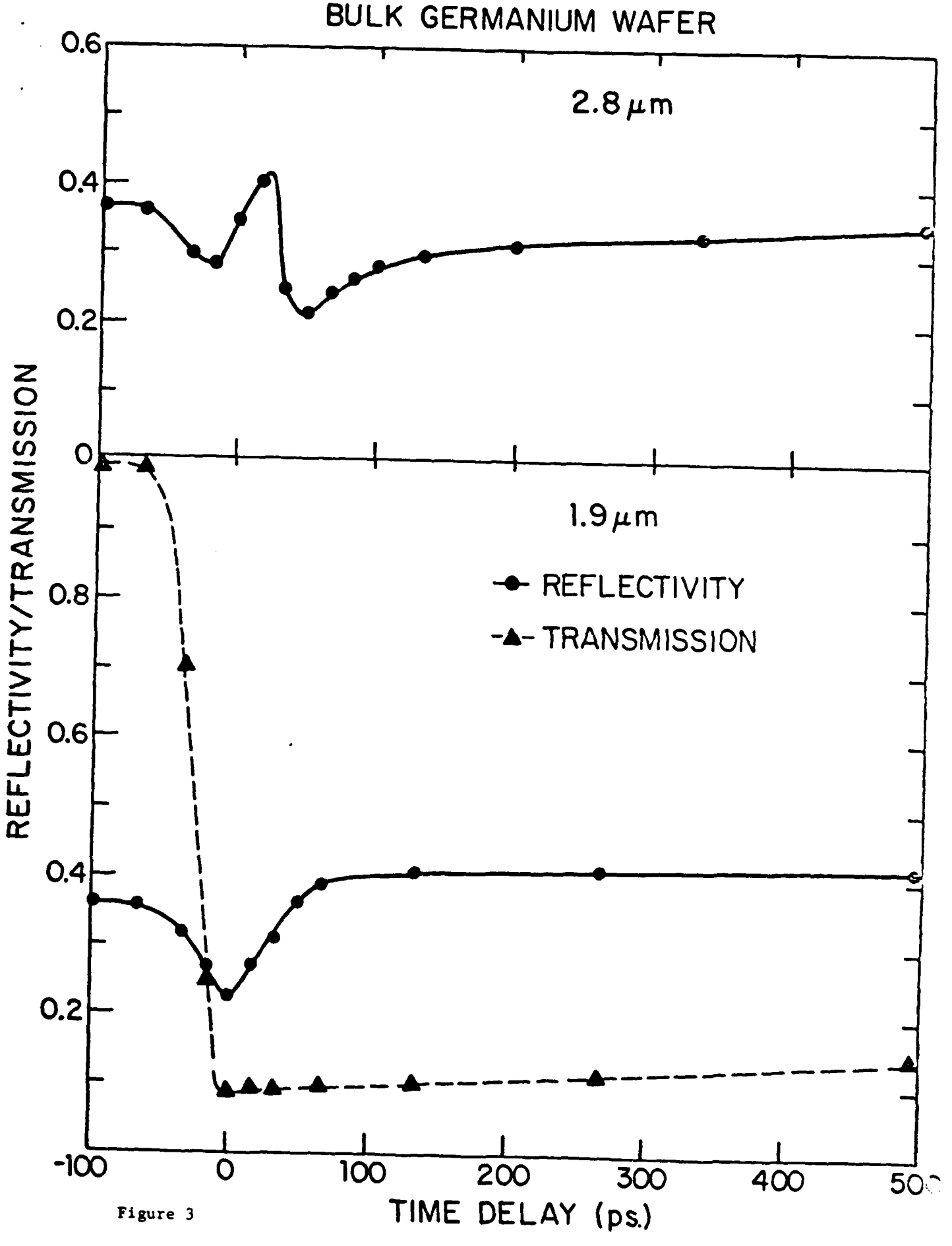
BULK GERMANIUM WAFER
2.8 μm
1.9 μm
REFLECTIVITY
TRANSMISSION
REFLECTIVITY/TRANSMISSION
TIME DELAY (ps.)
0.6
0.4
0.2
0
0.8
0.6
0.4
0.2
-100
0
100
200
300
400

Figure 3

Scripta METALLURGICA Vol. 17, pp. 1259-1262, 1983
Printed in the U.S.A.

SOLIDIFICATION MORPHOLOGY OF PICOSECOND PULSED LASER QUENCHED $Fe_{96}B_4$

Chien-Jung Lin and Frans Spaepen
Division of Applied Sciences, Harvard University, Cambridge MA 02138

(Received August 16, 1983)

Introduction

It is well known that the formation of metallic glasses from the melt is a configurational freezing process and that the glass transition is a kinetic phenomenon. Accordingly, for any given alloy, glass formation depends on the cooling rate used. In previous work, we have shown that the conventional glass formation ranges can be greatly extended by picosecond pulsed laser induced self-quenching. For instance, the glass formation range of picosecond laser quenched Ni-Nb alloys (1) is nearly double that achieved by splat-cooling (2); Fe-B alloys can be laser quenched into glasses with a B concentration as low as 5 at.% (3), which is significantly below the 12 at.% B minimum required for glass formation in melt-spinning (4).

We report here an interesting solidification morphology obtained by picosecond pulsed laser irradiation of Fe-B alloy containing about 4 at.% B.

Experimental Procedure

Details of the experimental procedure have been published previously (3). Briefly, sputtered compositionally modulated films of $Fe_{76}B_{24}$/Fe were used. The modulation wavelengths of these films were kept at about 2 nm to insure the homogeneity of the melt by mixing in the liquid state during the short lifetime of the melt (~1 ns) following a 30 psec laser pulse. The irradiation was performed in air, using a 1.06 μm Nd:YAG laser. Transmission electron microscopy and diffraction were used to characterize the microstructure after solidification.

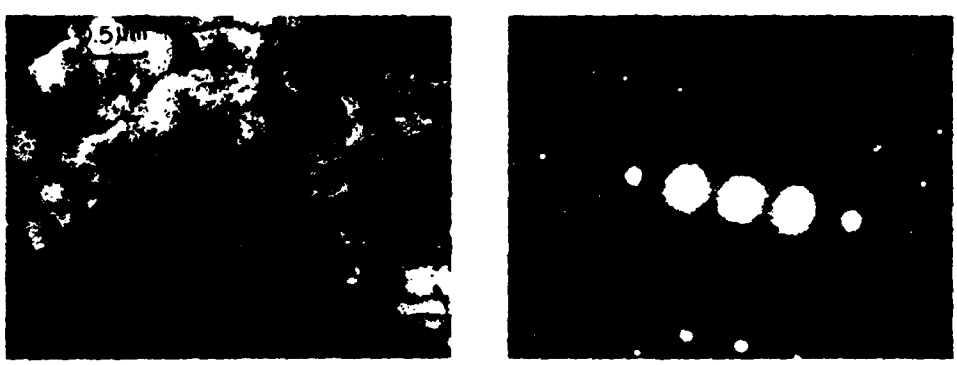

Fig. 1. TEM bright field micrograph and corresponding diffraction pattern from a $Fe_{95.5}B_{4.5}$ film after laser irradiation.

0036-9748/83 $3.00 + .00

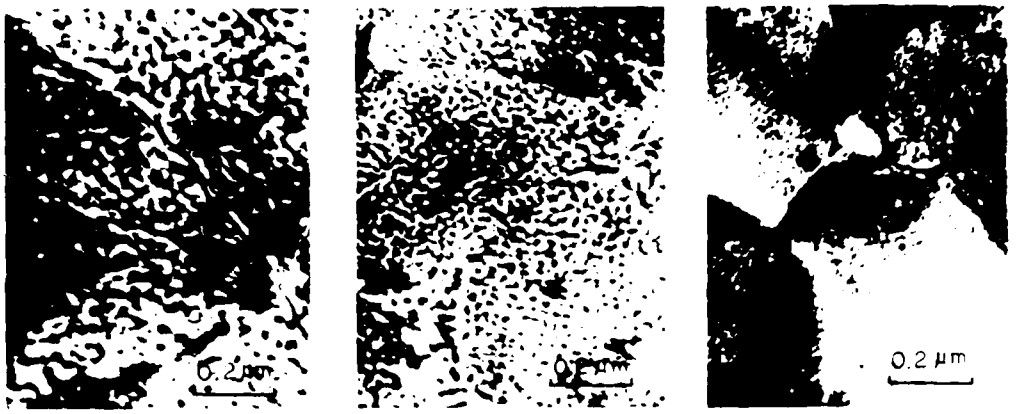

(a) (b) (c)

Fig. 2. TEM bright field micrographs of different regions of a laser irradiated spot in a $Fe_{96}B_4$ film: (a) center, (b) intermediate, (c) edge.

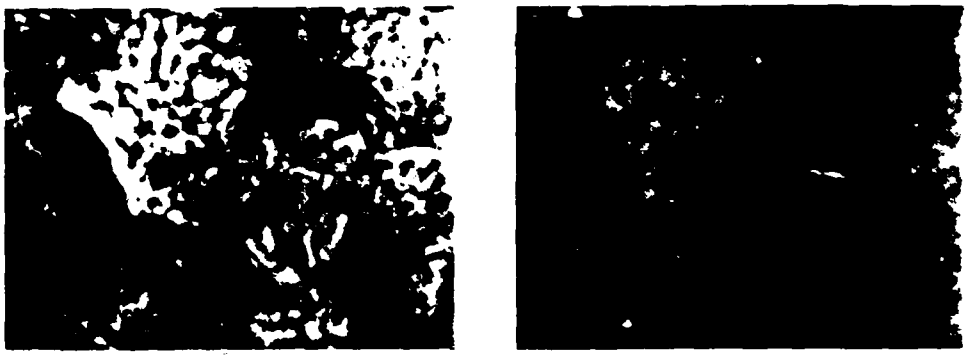

(a) (b)

Fig. 3. TEM bright field micrograph (a) and corresponding dark field micrograph (from the amorphous halo) (b), from a $Fe_{96}B_4$ film after laser irradiation

Results

Figure 1 shows the TEM bright field micrograph of $Fe_{95.5}B_{4.5}$ after irradiation; notice the fine features (10 nm) inside the 2-3 μm diameter b.c.c. grain. The selected area diffraction pattern shows single crystalline spots surrounded by several amorphous halos as a result of double diffraction. These features were also observed in psec laser quenched $Fe_{96}B_4$ films. Figure 2 shows a gradual decrease in the characteristic length scale of these features from the center (30 nm) toward the edge (5 nm) of the laser-irradiated spot. Interestingly, in a dark field micrograph from the halo, the contrast of these features is reversed (Figure 3), suggesting that it is due to a crystalline-amorphous phase difference. Furthermore, STEM microdiffraction

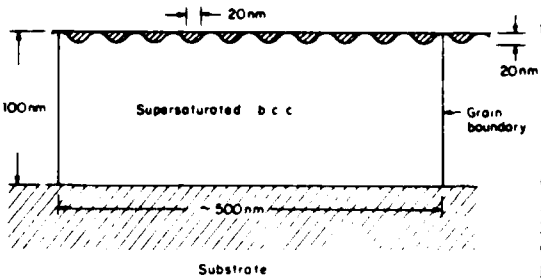

Fig. 4. Schematic illustration of the solidification morphology of a $Fe_{96}B_4$ film after laser irradiation.

patterns from both bright and dark regions of the same grain in Figure 3(a) showed the same single crystalline pattern.

Discussion

We suggest the following solidification mechanism, shown schematically in Figure 4, to explain these unusual morphologies. The b.c.c. crystals are thought to grow very rapidly after nucleation, up to several hundred meters per second (5), in the direction parallel to the surface until limited by mutual impingement. In the normal direction, the crystals are thought to grow initially fast enough to keep a stable planar growth front. As the growth front approaches the surface, it continually slows down, due to the decreasing thermal gradient. At some point, the crystal growth velocity may become low enough for morphological instability to set in (6,7). Crystalline protrusions develop on the growth front and reach the surface, while the regions between those protrusions become richer in B and hence quench into the glassy state. The characteristic length scale of the instability should depend on the growth front velocity (6), with the slower velocities giving larger features.

This mechanism accounts qualitatively for our observations:

(i) The amorphous phase in Figure 4 is confined to a layer of thickness similar to the characteristic length in the lateral direction. This is consistent with the STEM microdiffraction observations of the same single crystalline diffraction spots in the light or dark areas of the same grain. If the amorphous phase were dispersed throughout the 100 nm thick film, the 5-30 nm features would not be as clearly separated on the micrographs of Figure 2.

(ii) The melt depth at the edge of the irradiated spot is shallower, resulting in a steeper thermal gradient, a faster cooling rate, and a higher regrowth velocity (8); this explains the decrease of the characteristic length on Figures 2(a)-2(c).

(iii) The degree of segregation of B should be quite small, since it is limited by the very fast crystal growth rates. Accordingly, this solidification morphology is expected to occur only for alloys containing slightly less than 5 at.% B. At or above 5 at.% B, the cooling rate is high enough to make the entire sample glassy. Far below 5 at.% B, the amount of B is too small, either for constitutional undercooling to be effective, or for the B-rich regions to reach the minimum 5 at.% required for glass formation; indeed, we observe that all Fe-B alloys containing 3 at.% or less B become entirely crystalline (supersaturated b.c.c.).

We think it unlikely that the morphology is the result of equilibrium phase separation in the liquid state, since it is very difficult to reconcile the existence of a liquid miscibility gap with a T_o-composition (i.e., equal free energies for crystal and liquid) of 16 at.% B at 660K (5).

The dependence of the scale of the microstructure on the quench rate (see Figure 3) clearly establishes that the morphology is a result of the solidification process and not of a subsequent surface reaction. The short lifetime of the melt (1 ns) also rules out oxygen contamination from the air during irradiation. Possible contamination due to a pre-existing surface oxide can not explain the morphology, since the surface would be uniformly affected. At the power level used here, some evaporation occurs at the center of the spot, which cleans off the surface (9); nevertheless, the morphology is observed over the entire laser spot. STEM analysis also excluded contamination of the sample by the substrate (e.g. Al (3)) as a possible factor.

Conclusions

Compositionally modulated films with average composition $Fe_{96}B_4$ were irradiated by a 30 picosecond laser pulse. The solidification morphology showed a glassy region, with dimensions much smaller than the grain size, superimposed on the individual grains. This morphology is thought to result from an interfacial instability occuring at the last stages of the very fast crystal regrowth process.

Acknowledgment

The authors thank Dr. A.-L. Lompré for his help with the laser irradiation. The STEM work was done at the MIT Center for Materials Science; we thank Dr. A. Garratt-Reed for his assistance. This research was supported by the Office of Naval Research under contract no. N00014-83-K-0030.

References

1. C.-J. Lin and F. Spaepen (to be published).
2. R. C. Ruhl, B. C. Giessen, M. Cohen and N. Grant, Acta Met. 15, 1693 (1967).
3. C.-J. Lin and F. Spaepen, Appl. Phys. Lett. 41, 721 (1982).
4. R. Hasegawa and R. Ray, J. Appl. Phys. 49, 4174 (1978).
5. C.-J. Lin and F. Spaepen, in Chemistry and Physics of Rapidly Solidified Materials, edited by B. J. Berkowitz and R. Scattergood, TMS-AIME Conference Proceedings (in press).
6. J. W. Cahn, S. R. Coriell and W. J. Boettinger, in Laser and Electron Beam Processing of Materials, edited by C. W. White and P. S. Peercy, p. 89, Academic Press, New York (1980).
7. W. W. Mullins and R. F. Serkerka, J. Appl. Phys. 35, 444 (1964).
8. F. Spaepen and D. Turnbull, in Laser Annealing of Semiconductors, edited by J. M. Poate and J. W. Mayer, p. 15, Academic Press, New York (1982).
9. J. M. Liu, R. Yen, E. P. Donovan, N. Bloembergen and R. T. Hodgson, Appl. Phys. Lett. 38, 617 (1981).

Proceedings of 5th Int. Conf.
on Liquid and Amorphous Metals,
to appear in J. Non-Cryst. Solids.

PICOSECOND PULSED LASER-INDUCED MELTING AND GLASS FORMATION IN METALS

Chien-Jung Lin, Frans Spaepen and David Turnbull
Div. of Applied Sciences, Harvard University, Cambridge, Mass. 02138

ABSTRACT

Irradiation of a solid surface by a picosecond laser pulse leads to melting of a thin overlay, and subsequent quenching at rates of $\underline{10^{12}}$ $\underline{K/s}$ or higher. This technique is also one of the few available for superheating a crystal above its melting temperature. The ultra-fast quenching rates permit the formation of new metallic glasses. Work on the Fe-B and Ni-Nb system is reviewed, and new results on the Mo-Ni, Mo-Co and Nb-Co systems are reported. In all cases, glasses are formed below the T_o-line, indicating that partitionless crystallization is usually at least partially diffusion controlled due to the change in short range order upon crystallization; only in the simplest structures, such as disordered f.c.c. solutions, are the partitionless crystallization kinetics fast enough to preclude glass formation.

INTRODUCTION

When a solid metallic surface is irradiated by a laser pulse of duration t_p, the energy is deposited in a layer of thickness α^{-1}, where α is the absorption coefficient; for metals, α^{-1} is on the order of 100Å. During the pulse, a layer of thickness $(2D_{th}t_p)^{1/2}$ is heated up by thermal conduction, where D_{th} is the thermal diffusivity. For metals, D_{th} is on the order of $0.5cm^2/sec$, which, for a 30ps pulse, corresponds to an initial heated layer of about 500Å thick. For a typical laser fluence of about 0.5 J/cm^2 and a metallic reflectivity, the temperature rise in this (molten) layer is estimated to be several thousand degrees. The fraction of the energy lost due to evaporation is small (<10%) since it is limited by the evaporation kinetics and the short duration of the process. The rest of the energy is conducted into the

bulk, leading to further melting to a total depth on the order of 1000Å. Further cooling then leads to resolidification of this layer, either by crystallization or glass formation. Heat flow calculations and direct observations of melting (e.g. in Si, using time-resolved reflectivity) show that the total lifetime of the melt for a 30ps pulse is about 1 ns;[1] given that the temperature drop is on the order of 10^3K, this corresponds to an average cooling rate during solidification on the order of 10^{12}K/s. Since most 'conventional' quenching techniques, such as melt spinning, produce cooling rates of about 10^6K/s, it is expected that pulsed laser quenching can lead to the formation of new metastable phases. A review of the fundamentals of pulsed laser interactions with solid surfaces has been given by Bloembergen.[2]

MELTING AND SOLIDIFICATION KINETICS

The general formalism of these transformations has been reviewed by Spaepen and Turnbull.[3,4] The velocity of the crystal-melt interface, u, may be approximated by:

$$u \simeq u_o \, (T_M - T_i)/T_i \qquad (1)$$

where T_M is the melting temperature and T_i the temperature at the interface; u_o is a velocity determined by the kinetics of the melting or crystallization process: for pure metals, when these processes are collision-limited, u_o is approximately equal to the speed of sound, u_s; for alloys, where diffusive rearrangements may be important $u_o \simeq D/\lambda$ (D: diffusivity; λ: interatomic distance).

The heat flow associated with melting or solidification leads to a second expression for u:

$$u = - \kappa \bar{V} \nabla_i T / \Delta H_c \qquad (2)$$

with κ: thermal conductivity; $\bar{V}$: molar volume; $\nabla_i T$: temperature gradient at the interface; ΔH_c: molar heat of crystallization. The combination of eqs. (1) and (2) then leads to a determination of the interface temperature, T_i. If the interface kinetics are fast compared to the rate of heat removal (or heat supply, for melting), as is the case in most conventional metal processing, the process is called heat flow limited, and T_i is only slightly different from T_M. If, however, the interface kinetics are slow (e.g. if limited by diffusional rearrangements), and the rate of heat removal (or supply) is fast (e.g. due to the very steep thermal gradients in ps pulsed laser annealing), the process becomes interface limited, and T_i is very different from T_M.

If the kinetic processes at the interface are collision-limited, as in crystallization of pure metals, T_i differs from T_M by only a few tens of degrees even in ps pulsed laser quenching. It should be noted that the thermal gradients during the melt-in phase following the pulse are much steeper than during solidification: $\nabla_i T \simeq 10^3 K/(2D_{th}t_p)^{1/2} \simeq 10^{11} K/m$. According to eq. (2) this corresponds to a heat-flow limited velocity on the order of 2000m/s, i.e., on the same order of u_s. Eq. (1) therefore predicts a substantial overheat at the interface. Consequently, picosecond pulsed laser heating is one of the few methods available for superheating metallic crystals.

For metallic glass formation, it is clear that T_i must fall far below T_M during cooling, and that hence diffusion-limited interface kinetics seem required. The solidification velocity, u, in ps laser quenching can be estimated, from the melt depth (~1000Å) and the lifetime of the melt (~1 ns), to be at least 100m/s. The distance that an alloy atom can travel diffusively during the passing of the solidification front, $(D\lambda/u)^{1/2}$, is then less than

an interatomic distance. The solidification process is therefore a 'partitionless' one. Partitionless crystallization is only thermodynamically possible if the temperature drops below the so-called 'T_o-line' in Fig. 1, i.e., the line where the free energy of the crystal and the undercooled liquid solutions are equal.[5]

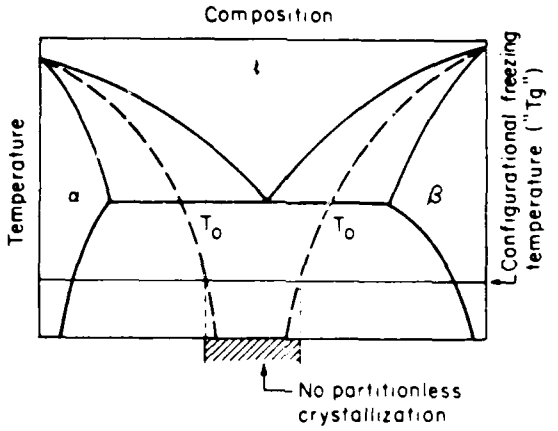

FIGURE 1
Schematic illustration of the T_o-lines (equal free energy for liquid and crystal) in a simple eutectic phase diagram.

This 'solute trapping' process has been discussed in detail by Aziz.[6] If the configurational freezing temperature ('T_g') of an alloy lies above the T_o-lines, glass formation is expected if no intermetallic phases can be formed; the complex structure of most of these phases, however, usually requires diffusion-like rearrangements that slow down the crystallization kinetics. Since partitionless crystallization into the primary solutions is often a very fast process, it has been proposed that the T_o-lines represent the limits of glass formation.[7,8] However, as will be demonstrated below, this is only the case for the simplest crystal structures, such as disordered f.c.c. alloys, where the kinetics may approach the collision limit. If, as is often the case, reconstruction of the short-range order is required, the cry-

stallization kinetics are at least partially diffusion-limited and glass formation can occur even below the T_o-lines.

EXPERIMENTAL PROCEDURE

The main experimental problem in studying the solidification of binary alloys in the ps pulse regime is obtaining a homogeneous melt in its 1 ns lifetime, since the mixing length corresponding to this time, $(Dt)^{1/2}$, is only 30Å. The phases in the alloy must therefore be dispersed on this scale. We have solved this problem[9,10] by preparing the starting alloy as a ~1000Å thick compositionally modulated film with a wavelength shorter than the mixing length. After irradiation, the film is floated off the substrate and is ready for transmission electron microscopy without further thinning. This procedure is also very flexible in that it allows preparation of a continuous range of compositions using only two sources or sputtering targets.

RESULTS

In earlier papers[9,10] we showed that Fe-B alloys with a B content as low as 5 at.% can be made glassy by psec laser quenching, whereas 'conventional' quenching requires a minimum of 12 at.%B. Below 5 at.%B, the alloys solidify as supersaturated b.c.c. crystals. Estimates of the T_o-line in the Fe-B system, based on regular solution modeling and on the devitrification mechanism, show that all the new alloys obtained by laser quenching were formed below the T_o-line.

Similar observations were made for the Ni-Nb system,[11] where glasses were formed by laser quenching in the 23-82 at.%Ni range, with (supersaturated) f.c.c. and b.c.c. crystalline solid solutions outside this range; the glass

formation range in 'conventional' quenching[12] is only 40-70 at.%Ni, and corresponds roughly to the range between the T_o-lines. Again, laser quenching demonstrated that glasses could still be formed far <u>below</u> the T_o-lines.

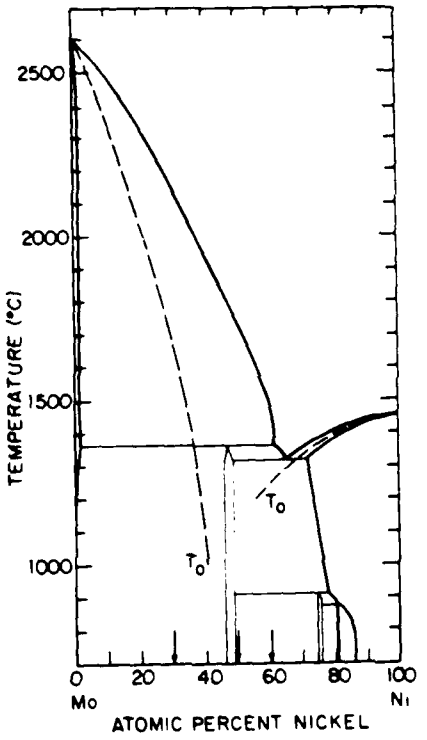

FIGURE 2
Molybdenum-nickel phase diagram, indicating estimated T_o-lines for the primary solid solutions. Glasses have been formed by laser irradiation at the three compositions indicated by arrows.

We also report here new results on glasses formed in the Ni-Mo, Co-Mo and Co-Nb systems. Figure 2 shows the Mo-Ni phase diagrams with estimated T_o-lines for the primary solid solutions. For three compositions, with 30, 50 and 60 at.%Ni, ps laser quenching produced the amorphous phase. Note that in two cases glasses are formed below the T_o-line, and that the δ(MoNi) intermetallic is not formed upon quenching the alloy between the T_o-lines. Similar alloys, with 35, 50 and 65 at.%Ni, had been made amorphous by Liu <u>et al</u>[13] by

ion mixing of multi-layer films of the crystalline elements. In the 60 at.%Ni alloy, we observed some microcrystals, but only near the center of the laser-irradiated spot; in the 30 at.%Ni alloy some crystals (b.c.c.) were observed at the edge of the spot, but not in the center; in the 50 at.%Ni alloy the entire spot was amorphous. A possible explanation of the difference in the occurrence of the crystals may be that crystals at the edge in the 30 at.%Ni alloys grow epitaxially on the only partly melted modulated film (the beam has a Gaussian intensity profile), whereas in the 60 at.%Ni alloy, the higher quench rate at the edge suppresses growth, while at the slower cooling center new crystals can nucleate on the substrate. Figures 3 and 4 show the diffraction patterns of as-deposited and irradiated $Mo_{55}Co_{45}$ and $Nb_{40}Co_{60}$ alloys. In both cases, fully glassy phases are formed upon irradiation. To our knowledge, Co-Mo amorphous alloys had so far not been produced by liquid quenching; Liu _et al_[13] have produced amorphous alloys with 65 and 35 at.%Co by ion mixing. It is interesting that the as-deposited modulated Nb-Co film is entirely amorphous, whereas the as-deposited Mo-Co film is entirely crystalline, although both were prepared by sequential sputter deposition of the crystalline elements. Since both systems are clearly glass formers, and since the sputter-induced mixing is probably similar for both films, the occurrence of the as-deposited amorphous film may be the result of enhanced solid state interdiffusion between the layers, as observed in La-Au.[14]

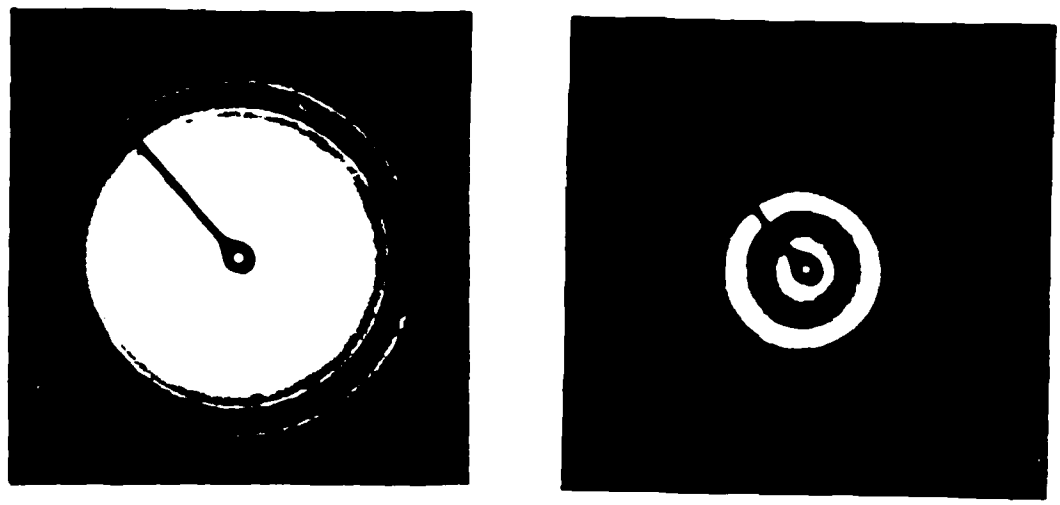

FIGURE 3
Electron diffraction patterns of an as-deposited (a) and laser-irradiated (b) compositionally modulated film of average composition $Mo_{55}Co_{45}$.

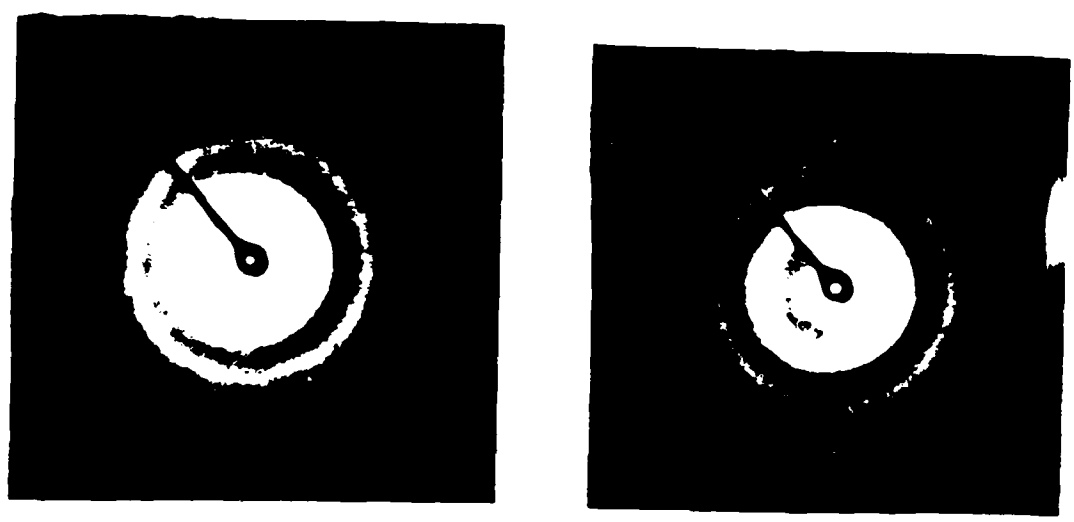

FIGURE 4
Electron diffraction patterns of an as-deposited (a) and laser-irradiated (b) compositionally modulated film of average composition $Nb_{40}Co_{60}$.

ACKNOWLEDGEMENTS

This work has been supported by the Office of Naval Research under Contract No. N00014-83-K-030.

REFERENCES

1) J.M. Liu, Thesis, Harvard University, 1982.

2) N. Bloembergen, in: Laser-Solid Interactions and Laser Processing, eds. S.D. Ferris, H.J. Leamy and J.M. Poate (AIP, New York (1979). p. 1.

3) F. Spaepen and D. Turnbull, ibid., p. 73.

4) F. Spaepen and D. Turnbull, in: Laser Annealing of Semiconductors, eds. J.M. Poate and J.W. Mayer (Academic Press, New York, 1982) p. 15.

5) J.C. Baker and J.W. Cahn, in: Solidification, eds. T.J. Hughel and G.F. Bolling (ASM, Metals Park, Ohio, 1971), p. 23.

6) M.J. Aziz, J. of Appl. Phys. 53, 1158 (1982).

7) T.B. Massalski, in: Proc. 4th Int. Conf. on Rapidly Quenched Metals, eds. T. Masumoto and K. Suzuki (Jap. Inst. Metals, 1982), p. 203.

8) W.J. Boettinger, ibid., p. 99.

9) C.-J. Lin and F. Spaepen, Appl. Phys. Lett. 41, 721 (1982).

10) C.-J. Lin and F. Spaepen, in: Chemistry and Physics of Rapidly Solidified Materials, eds. B.J. Berkowitz and R. Scattergood, TMS-AIME Symposia Proc., in press.

11) C.-J. Lin and F. Spaepen, submitted to Acta Met.

12) R.C. Ruhl, B.C. Giessen, M. Cohen and N. Grant, Acta Met. 15, 1693 (1967).

13) B.X. Liu, W.L. Johnson, M.A. Nicolet and S.S. Lau, Appl. Phys. Lett. 42, 45 (1983).

14) R.B. Schwarz, W.L. Johnson, and B.M. Clemens, this volume.

METALLIC GLASSES AND METASTABLE CRYSTALLINE PHASES PRODUCED BY PICOSECOND PULSED LASER QUENCHING

C.-J. LIN[†] AND F. SPAEPEN
Division of Applied Sciences, Harvard University, Cambridge, MA 02138

ABSTRACT

The mechanism of ultrafast cooling (10^{12}K sec^{-1}) by picosecond pulsed laser irradiation is reviewed, and it is demonstrated that only partitionless transformations can occur. The glass formation range in a number of binary systems is reviewed, demonstrating that many glasses can be formed below the T_0-line. The formation of metastable crystalline alloys in the Fe-B, Ni-Nb, Cu-Co and Au-Co systems is reported.

INTRODUCTION

As discussed in detail by Bloembergen [1] and others [2-3], picosecond pulsed lasers can be used to induce very high quench rates, up to 10^{12}K/sec., in thin molten overlays on a metallic substrate. Figure 1 illustrates the stages of this process: (i) energy deposition in a layer on the order of the absorption depth (~500Å); (ii) very fast melting (~1000m/sec.) of a ~1000Å thick layer; (iii) cooling, accompanied by fast crystal regrowth (~100m/sec.) or glass formation.

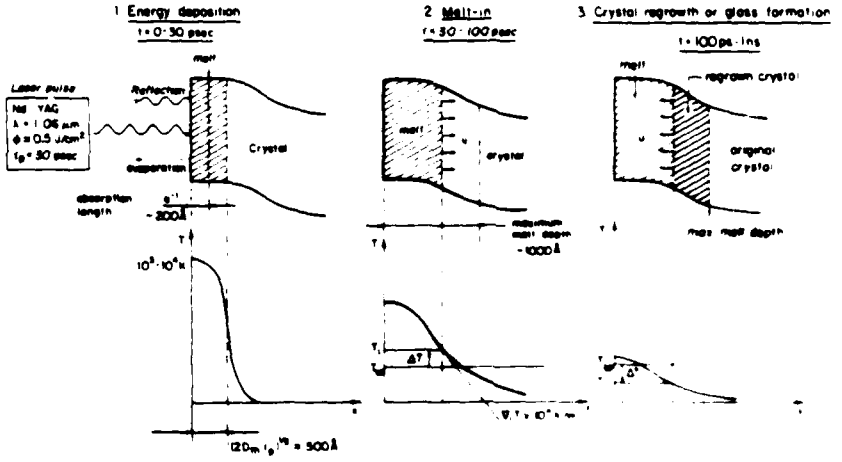

FIG. 1. Schematic diagrams illustrating the [illegible] quenching.

The crystal growth or melting velocity, v, is determined by the [illegible] balance:

$$v = \frac{}{H_f}$$

(K: thermal conductivity; $\nabla_i T$: temperature gradient difference at the interface; $\bar{V}$: molar volume; ΔH_f: molar heat of fusion), and by the kinetics of interface motion:

$$u \simeq u_o \frac{T_M - T_i}{T_i} \qquad (2)$$

(T_M: melting temperature; T_i: interface temperature; u_o: velocity prefactor).

For collision-limited motion $u_o \approx u_s$, the speed of sound; for diffusion-limited motion $u_o \simeq D/\lambda$ (D: diffusivity in the liquid; λ: interatomic distance); a mixed mechanism has a value of u_o between these two. Since the temperature gradients in this process are very steep (10^{11}K/m in melting; 10^{10}K/m in cooling), equating u in Eqs. (1) and (2) leads to values of T_i that are considerably different from T_M. Upon cooling, this can lead to the formation of new metastable crystalline phases, or, if the crystal growth kinetics are slow enough, glass formation. The lifetime of the melt, determined experimentally on Si [4,5] or estimated from heat flow calculations, is about 1 ns under the conditions described above. Since the temperature of the material changes on the order of several thousand degrees in that amount of time, the cooling rate must be at least $\dot{T} = 10^3\text{K}/10^{-9}\text{sec} = 10^{12}\text{K/sec}$.

EFFECT OF EVAPORATION

An aspect of the irradiation process that has so far not been considered in detail is the loss of matter and energy by evaporation. However, even if the liquid is overheated far above its boiling point, the evaporation rate, estimated from kinetic gas theory, is only on the order of 10^{11} monolayers per second for typical metals. During the lifetime of the melt, this amounts to a loss of material of, at most, a few tens of monolayers; for the same reason, the loss of energy due to evaporation is at most on the order 10^8W.cm^{-2} (at 10,000K), which is negligible compared to the laser intensity of at least 10^9W.cm^{-2}. We have checked the accuracy of these estimates experimentally by measuring the recoil pressure of evaporation (equal to half the equilibrium vapor pressure), by observing the amplitude of oscillation of a thin metallic ribbon, clamped at one end and irradiated with the laser pulse at the free end. A recoil pressure on the order of 10^{10}Nm^{-2} was observed, which is indeed of the same order as the equilibrium vapor pressure around 10^4K.

The holes often found after irradiation with a Gaussian beam are the result of the *mechanical* displacement of the liquid ("splashing") by this large recoil pressure; they are *not* a result of direct evaporation. Most of our experiments were performed on a layer supported by an aluminum film (see below); if a hole was found as a result of irradiation, sometimes traces of Al were observed on the top of the surface in the immediate vicinity of the hole, this can only be explained by "splashing".

Another consequence of the inefficient rate of energy removal by evaporation is that increasing the laser fluence mostly leads to further overheating of the liquid; too large a fluence, therefore results in a deeper melt and a lower quench rate.

EXPERIMENTAL METHODS

Since the lifetime of the melt, t, in our experiments is only 1 ns, the mixing length, $(Dt)^{1/2}$, in the melt for a diffusivity $D = 10^{-4}\text{cm}^2\text{sec}^{-1}$ is

only about 30Å. When studying multiphase alloys, the starting materials must therefore be dispersed on a scale finer than this length. We accomplished this by using ~1000Å thick compositionally modulated films, produced by sequential deposition, with a modulation wavelength of about 20Å [5]. These films were deposited on a 1 μm thick aluminum layer supported by a copper substrate. The aluminum layer acts as a heat sink, and its dissolution in dilute NaOH allows the irradiated layer to be floated off; the entire irradiated spot can then be examined by transmission electron microscopy without any further thinning.

TRANSFORMATIONS

Since the solidification velocity, u, during cooling of the melt is on the order of 100 m/sec., the time required to solidify one monolayer, λ/u, is on the order of 1 ps. The distance that an alloy atom can travel diffusively in that amount of time, $(D\lambda/u)^{1/2}$, is then less than an interatomic distance. The only transformations that can occur under these conditions are therefore partitionless crystallization or, if the crystal growth kinetics are slow enough, glass formation. Figure 2 illustrates the transformation products for a number of binary metallic systems.

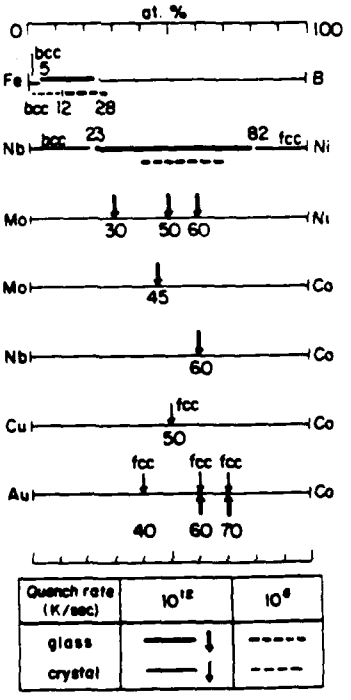

FIG. 2. Comparison of the alloy phases formed by conventional quenching (10^6K/sec.) and picosecond pulsed laser quenching (10^{12}K/sec.).

Glass Formation

We have previously reported [3,5,6,7] a number of results on the binary metallic glasses listed on Fig. 2. It is clear that the glass formation composition range is extended greatly beyond that of conventional methods. For example, in the Ni-Nb system [8], the glass formation range for laser

quenching is very close to that for sputter-quenching [9], which is remarkable, given the very different mechanisms of formation. Many of the glasses were formed below the so-called "T_o-line" in the phase diagram [10], which is the region where partitionless crystallization is possible as well. This shows that the kinetics of partitionless crystallization are not necessarily very fast (collision limited), since changes in short-range order upon crystallization may require diffusional rearrangements. For the composition of a system to lie entirely above the T_o-lines is therefore a *sufficient* condition for glass formation under these conditions (excluding intermetallic formation), but it is not a necessary one as has been claimed [11,12]. The same diffusional short range order change must be invoked to explain the stability of glasses below the T_o-line after formation.

Crystalline Phases

A number of the binary systems on Figure 2 have equilibrium intermetallic phases at compositions that were laser quenched. None of them, however, were observed in the transformation products. This is most likely the result of their rather complex crystal structure, formation of which requires extensive local diffusional rearrangements. For example, the equilibrium phase of $Mo_{50}Ni_{50}$ is the δ-phase, which is a Frank-Kasper phase with 56 atoms per unit cell; upon laser-quenching only glass was formed.

The only crystalline phases with growth kinetics that are fast enough to prevent glass formation have simple crystal structures: dilute b.c.c. solutions (Fe with up to 4%B, Nb with up to 18%Ni) and disordered f.c.c. solutions (Ni with up to 11%Nb, $Cu_{50}Co_{50}$, and Au with 40, 60 and 70%Co). The Ni alloys were heavily faulted and twinned, as were all f.c.c. pure metals and alloys, with the exception of pure gold. Figure 3 (a-d) shows micrographs and diffraction patterns of the $Cu_{50}Co_{50}$ alloy before and after quenching. The increase in grain size upon regrowth was observed in most other cases where crystalline phases were formed (e.g. pure Fe or Fe(B) [7]). Exceptions are the Au-Co alloys in which microcrystals were formed (<100Å). In the 30 and 40%Au systems a small amount of glassy phase seemed to be present as well. The fine features of the diffraction pattern of Figure 3d result from the extensive faulting in the system.

Although it has long been known that f.c.c. solid solutions can be made in the Cu-Ag system at all compositions [13], we quenched alloys with 35, 50 and 65 at%Ag to check the homogeneity of the melt formed from the modulated film; the sharpness of the diffraction ring of the solid solution demonstrated perfect homogeneity.

In compositions near the glass formation range, morphological instabilities in the latter stage of solidification (when the growth velocity is much slower) can lead to the formation of a two-phase crystalline-amorphous microstructure due to the enrichment of one phase by rejection of impurity. This has been observed in the $Fe_{96}B_4$ system [7].

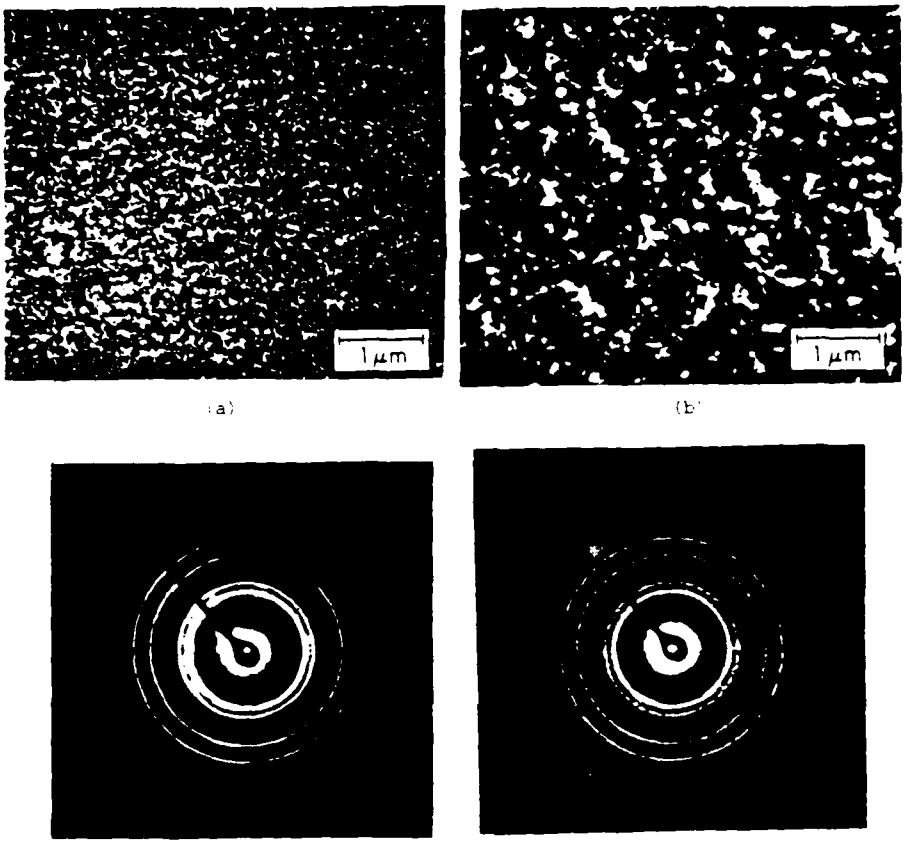

Fig. 4. Comparison of the dark field images and diffraction patterns of [illegible] before (a), (c) and after (b), (d) picosecond pulsed laser irradiation.

ACKNOWLEDGMENT

This work has been supported by the Office of Naval Research under Contract No. N[illegible] 14-83-K-[illegible].

REFERENCES

1. N. Bloembergen, in: Laser-Solid Interactions and Laser Processing, eds. S.D. Ferris, H.J. Leamy, and J.M. Poate, A.I.P., New York (1979), p. 1.
2. F. Spaepen and D. Turnbull, in: Laser Annealing of Semiconductors, eds. J.M. Poate and J.W. Mayer, Academic, New York (1982), p. 15.
3. C.-J. Lin, F. Spaepen and D. Turnbull, Proc. 5th Int. Conf. on Liquid and Amorphous Metals: J. Non-Cryst. Sol., in press.
4. J.M. Liu, Thesis, Harvard University, 1981.
5. C.-J. Lin and F. Spaepen, Appl. Phys. Lett., 41, 721 (1982).
6. C.-J. Lin and F. Spaepen, in: Chemistry and Physics of Rapidly Solidi-

fied Materials, eds. B.J. Berkowitz and R. Scattergood, TMS-AIME, New York (1983), p. 273.
7. C.-J. Lin and F. Spaepen, Scripta Met., 17, 1259 (1983).
8. C.-J. Lin and F. Spaepen, to be published.
9. T.W. Barbee, W.H. Holmes, D.L. Keith, M.K. Pyzyna, and G. Ilonca, Thin Sol. Films, 45, 591 (1977).
10. J.C. Baker and J.W. Cahn, in: Solidification, eds. T.J. Hughel and G.F. Bolling, ASM, Metals Park, Ohio (1971), p. 23.
11. T.B. Massalski, Proc. 4th Int. Conf. on Rapidly Quenched Metals, eds. T. Masumoto and T. Suzuki, Jap. Inst. Metals (1982), p. 203.
12. W.J. Boettinger, ibid., p. 99.
13. P. Duwez, R.H. Willens, and W. Klement, Jr., J. Appl. Phys., 31, 1136 (1960).

†Present address: IBM Research Laboratory, 5600 Cottle Road, San Jose, CA 95193.

MRL

Fe-B glasses formed by picosecond pulsed laser quenching

Chien-Jung Lin and Frans Spaepen
Division of Applied Sciences, Harvard University, Cambridge, Massachusetts 01238

(Received 14 June 1982; accepted for publication 4 August 1982)

Using picosecond pulsed laser irradiation, Fe-B alloys have been melted and quenched into glasses, with a B content as low as 5 at. %, which is significantly less than the minimum 12-at. % B content required for glass formation by other liquid quenching techniques. Compositionally modulated films with wavelengths on the order of 20 Å were used as starting materials to ensure homogeneity of the melt after irradiation.

PACS numbers: 64.70.Kb, 61.40.Df, 81.20.Pe, 42.60. – v

Since the first successful formation of Au-Si metallic glass by quenching from the liquid,[1] a large number of metallic alloys have been prepared as glasses. It is now widely believed that nearly all liquids would undergo a transition to a glassy state provided that crystallization can be bypassed during cooling.[2] To bypass crystallization, dramatically different cooling rates are required for different metallic alloys. Pure monatomic metals are believed to be the most difficult glass formers.[3] The cooling rates achieved by the socalled "splat-quenching" or "melt-spinning" techniques, in which a liquid is spread as a thin layer over a cold substrate, range from 10^5 to 10^8 K/s.[4] These techniques can form metallic glasses only for selected alloy systems and only over limited composition ranges. For example, Fe-B alloys can be made into glasses by splat quenching only if they contain 12–28 at. % B.[5] Below 12 at. % B metastable bcc crystalline solid solutions are formed.[6]

Pulsed lasers have been used to study rapid melting and resolidification in surface layers of semiconductors and metals. Very short duration laser pulses can induce much higher cooling rates than those achieved by splat quenching (10^{10} K/s for nanosecond pulses[7] and 10^{11} K/s for picosecond pulses[8]). These ultrahigh quenching rates make it possible to study new regimes of crystal growth and glass formation kinetics, and to form new metastable phases. For example, Liu *et al.*[9] used picosecond pulsed laser irradiation to form the amorphous semiconductor phase of Si from the melt, whereas other liquid quenching techniques always produce the stable crystalline phase. In this letter, we report on the glass formability of low B containing Fe-B alloys under these ultrafast quenching conditions. To our knowledge, these are the first experiments on metallic glass formation using picosecond pulsed irradiation.

A major problem in these picosecond pulsed laser experiments is obtaining a homogeneous melt within the very short time that the material is in the molten state. For example, experiments with 15-ps UV pulses on a silicon surface indicate that the lifetime of the melt is about 1 ns.[10] Since in these experiments the optical penetration depth is much shorter than the thermal diffusion length, the lifetime of the melt is determined mainly by the pulse duration and the thermal conductivity of the material.[8] Since the conditions for experiments on metals are similar, the melt lifetime is also expected to be about 1 ns for a 30-ps pulse. For a liquid diffusivity $D = 10^{-4}$ cm^2 s^{-1}, this corresponds to a mixing length ($\sqrt{Dt}$) of about 30 Å. The starting material for the experiment must therefore be homogeneous on this scale. This is a difficult requirement for two-phase alloys, such as Fe-B in the composition range of interest here. Ion implantation is one technique used to achieve alloy homogeneity.[11] We have chosen to make our starting alloys as compositionally modulated films, with modulation wavelengths on the order of the mixing length (16–35 Å), as illustrated by Fig. 1. The films consisted of multiple alternating layers of Fe and $Fe_{76}B_{24}$, sequentially sputter deposited[12,13] onto a water-cooled copper substrate coated by an evaporated Al film. The total film thickness was about 1000 Å. The average composition of the films could most reliably be obtained from the previously determined deposition rates of the Fe and $Fe_{76}B_{24}$ layers. The uncertainty for the composition is estimated to be less than 10% of the B content. No impurities could be detected by electron probe microanalysis (EPMA). An additional advantage of this modulated film technique, besides its relative simplicity, is its flexibility: it can be used for any alloy system, and can produce different compositions by varying the relative layer thicknesses. For example, in these experiments, alloys with average compositions in the range 0–24 at. % B have been made using only two targets (Fe, Fe_4B).

The samples were irradiated with 30-ps neodymium:yttrium aluminum garnet (Nd:YAG) laser pulses ($\lambda = 1.06$ μm). The beam had a Gaussian intensity profile, with a diameter of about 100 μm and an average fluence of 0.8 J/cm^2.

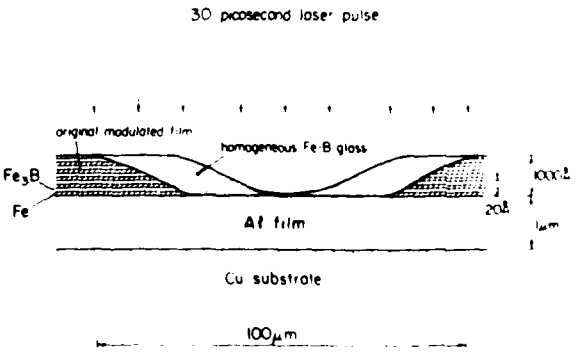

FIG. 1. Schematic cross section, drawn to a variable scale, of a compositionally modulated film after irradiation by a 30-ps laser pulse with a Gaussian intensity profile

 0003-6951/82/080721-03$01.00

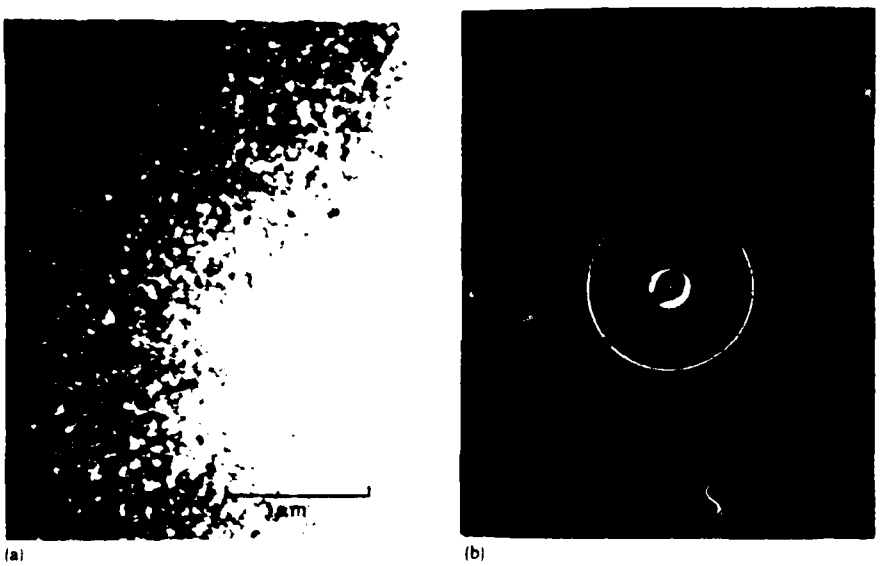

(a) (b)

FIG. 2. (a) TEM dark field image and (b) corresponding diffraction pattern from a $Fe_{76}B_{24}$ film before laser irradiation.

After irradiation, the films were taken off the substrates by dissolving the Al layer in dilute NaOH solution. Films prepared by this method can immediately be examined by transmission electron microscopy (TEM), without further thinning. This in turn allows a whole irradiated spot to be observed. The laser-irradiated regions can be easily distinguished in the TEM image by the disappearance of the "orange peel" morphology [see Fig. 2(a)], which is a replica of the substrate surface.

In the modulated films, the as-deposited $Fe_{76}B_{24}$ layers are amorphous, as shown by the weak halo superimposed on first diffraction ring of α-Fe in Fig. 2(b), and the as-deposited Fe layers consist of polycrystalline α-Fe with a grain size less than 100 Å. All the Fe-B alloys, with 24, 19, 15, 10, 8 and 5 at. % B, were found to form glasses, after irradiation, as shown in Figs. 3(a) and 3(b). Except for the 5-at. % B films, no epitaxial growth from pre-existing α-Fe crystals or nucleation of metastable crystalline phases could be observed anywhere in the laser-irradiated spot. Films containing only 5 at. % B, contained some large ($\sim$1000 Å) bcc crystals at the outer boundary of the irradiated regions. We could not determine whether the crystals were α-Fe or a metastable $Fe_{95}B_5$ bcc solid solution, since the difference in lattice spacing between them is very small (0.003 Å).[6] Most likely they are Fe_{95} B_5, since growth of α-Fe requires diffusion over a distance of about 1000 Å, which seems not plausible during the short lifetime of the melt. Since the lattice spacing of metastable bcc $Fe_{95}B_5$ is very close to that of α-Fe, it is quite possible that the bcc $Fe_{95}B_5$ crystals grew epitaxially from pre-existing α-Fe crystals, which are present only at the boundary of the irradiated spot.

It has been argued that the possibility of forming a crystalline phase of the same composition as the melt makes glass formation difficult, since partitionless crystallization (i.e.,

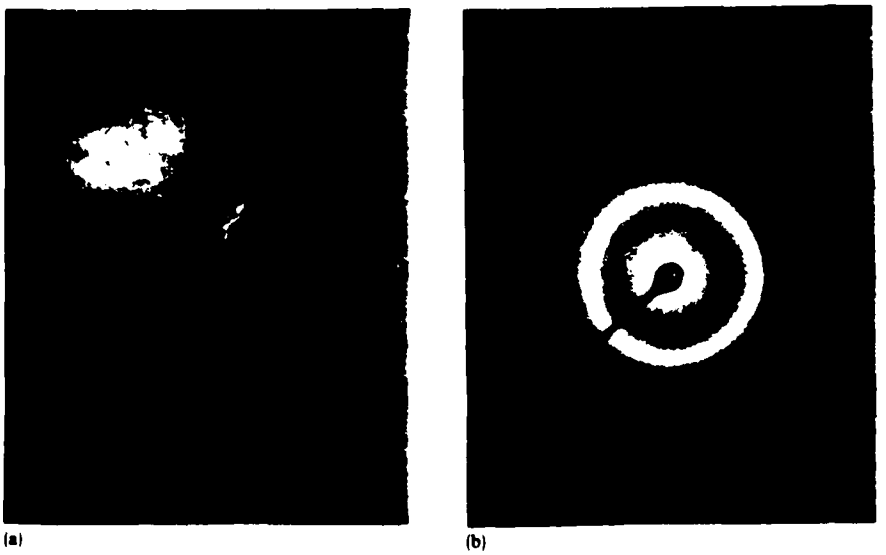

(a) (b)

FIG. 3. (a) TEM dark field image and (b) corresponding diffraction pattern from a $Fe_{76}B_{24}$ film after laser irradiation.

without solute redistribution) is thought to be a very fast process.[14,15] In the Fe-B system, however, alloys with a B content between 5 and 12 at. % can be quenched into glasses (at high enough rates) as well as solid solutions[6] (at lower quench rates). This indicates that, although crystallization is interface limited, the kinetic coefficient is much smaller than the collision-limited value,[16,17] presumably due to the local rearrangements required to change the strong chemical short range order around the B atom in the liquid state to that characteristic of the bcc solid solution. The same argument must also be invoked to account for the thermal stability of the glassy phase after the quench.

In conclusion, we have demonstrated that the ultrahigh cooling rate induced by picosecond laser pulse irradiation can be used to obtain glassy Fe-B alloys with a B content as low as 5 at. %, which is very significantly lower than the B content required for glass formation by other liquid quenching techniques. The cooling rates in these experiments are the highest ones used so far to quench liquids, and the results illustrate the potential of the technique for formation of new glasses and for the study of the kinetics of crystal growth.

The authors thank J. M. Liu for his help in the operation of the laser and Professor D. Turnbull for helpful discussions and a review of the manuscript. This research was supported in part by the National Science Foundation, Materials Research Grant (DMR 80-20247). C. J. L. acknowledges support by a predoctoral fellowship from the Exxon Corporation.

[1] W. Klement, R. H. Willens, and P. Duwez, Nature **187**, 869 (1960).
[2] M. H. Cohen and D. Turnbull, J. Chem. Phys. **31**, 1164 (1959).
[3] D. Turnbull, Contemp. Phys. **10**, 473 (1969).
[4] H. Jones, in *Proceedings of the 2nd International Conference on Rapidly Quenched Metals*, edited by N. J. Grant and B. C. Giessen (MIT, Cambridge, MA, 1976), p. 1.
[5] R. Hasegawa and Ranjan Ray, J. Appl. Phys. **49**, 4174 (1978).
[6] R. Ray and R. Hasegawa, Solid State Commun. **27**, 471 (1978).
[7] M. von Allmen, S. S. Lau, M. Maenpaa, and B-Y. Tsaur, Appl. Phys. Lett. **36**, 205 (1980).
[8] N. Bloembergen, in *Laser-Solid Interactions and Laser Processing*, edited by S. D. Ferris, H. J. Leamy, and J. M. Poate (AIP, New York, 1978), p. 1.
[9] P. L. Liu, R. Yen, N. Bloembergen, and R. T. Hodgson, Appl. Phys. Lett. **34**, 864 (1979).
[10] J. M. Liu, H. Kurz, and N. Bloembergen (unpublished).
[11] S. T. Picraux, D. M. Follstaedt, J. A. Knapp, W. R. Wampler, and F. Rimini, in *Laser and Electron Beam Processing of Materials*, edited by J. F. Gibbons, L. D. Hess, and T. W. Sigmon (North-Holland, Amsterdam, 1981), p. 575.
[12] M. P. Rosenblum, F. Spaepen, and D. Turnbull, Appl. Phys. Lett. **37**, 184 (1980).
[13] A. L. Greer, C.-J. Lin, and F. Spaepen, in *Proceedings of the 4th International Conference on Rapidly Quenched Metals*, edited by T. Masumoto and K. Suzuki (Japan Institute of Metals, Japan, 1982), Vol. I, p. 567.
[14] W. J. Boettinger, in *Proceedings of the 4th International Conference on Rapidly Quenched Metals*, edited by T. Masumoto and K. Suzuki (Japan Institute of Metals, Japan, 1982), Vol. I, p. 99.
[15] T. B. Massalski, in *Proceedings of the 4th International Conference on Rapidly Quenched Metals*, edited by T. Masumoto and K. Suzuki (Japan Institute of Metals, Japan, 1982), Vol. I, p. 203.
[16] F. Spaepen and D. Turnbull, in *Laser-Solid Interactions and Laser Processing*, edited by S. D. Ferris, H. J. Leamy, and J. M. Poate (AIP, New York, 1979), p. 73.
[17] F. Spaepen and D. Turnbull, in *Laser Annealing of Semiconductors*, edited by J. M. Poate and J. W. Mayer (Academic, New York, 1982), Chap. 2.

MRL

In *Chemistry and Physics of Rapidly Solidified Materials*, B.J. Berkowitz and R.O. Scattergood, Eds., 1983.

Fe-B GLASSES FORMED BY PICOSECOND PULSED LASER QUENCHING

[illegible] Lin* and Frans Spaepen

[illegible] of Applied Sciences
Harvard University
Cambridge, Massachusetts 02138
U.S.A.

[illegible] pulsed laser beam can be used to melt surface layers [illegible] of crystalline alloys, subsequently cool very rapidly (up to 10^{12} K s^{-1}), and thereby quench the liquid into the metallic glass state. Using this technique, Fe-B [illegible] alloys with a B content as low as 7 at.% have been produced, whereas [illegible] liquid quenching techniques require a minimum boron content of 11 at.% to [illegible] glass formation.

The short temperature [illegible] of the melt during the 1 nsec lifetime of the [illegible] experiments were performed on sputter-deposited compositionally modulated Fe/Fe$_x$B$_{1-x}$ films, with a modulation wavelength on the order of the nearest neighbor distance, $\lambda \approx 2$ Å.

The main competing process for glass formation in the low-B composition [illegible] is partitionless crystal growth of a supersaturated α-Fe(B) solution, as observed in conventional quenching processes. Thermodynamic estimates of the [illegible] in the Fe-B phase diagram confirm this. Although partitionless crystal growth is potentially a very fast mechanism (e.g. in pure Fe), in these Fe-B alloys it is probably slowed down by the reconstruction required to change the chemical short range order around the B-atom upon crystallization.

* Exxon Predoctoral Fellow

Introduction.

Since the first successful quenching of liquid Au_4Si to the glassy state (1), many metallic alloys have been prepared as glasses. As proposed by Cohen and Turnbull (2), it appears that nearly all liquids would undergo a transition to a glassy state if crystallization can be bypassed on cooling. This condition is most difficult to meet in pure monatomic metals, which are therefore believed to be the most difficult glass formers (3).

The cooling rates achieved by the so-called 'splat-quenching' or 'melt-spinning' techniques, in which a liquid is spread as a thin layer over a cold substrate, range from 10^5 to 10^8 K/s (4). Only selected alloy systems, over limited composition ranges, can be quenched into glasses at these cooling rates. For example, Fe-B alloy glasses can be produced by splat-quenching only if they contain 12-28 at.% B (5). Below 12 at.%B, metastable bcc crystalline solid solutions are formed (6).

It is well known that short laser pulses can induce rapid melting and resolidification in surface layers of semiconductors and metals. The shorter the pulse duration, the faster the heating and cooling. With [illegible] pulses, ultrafast cooling, up to 10^{13} K/s, can be achieved (7). These ultrahigh quenching rates make it possible to study new regimes of crystal growth, formation of metastable phases, and glass-forming kinetics. The usefulness of these ultrahigh quenching rates has been demonstrated by the work of Liu et al (8), who used 1 psec U.V. pulses to melt Si and subsequently form its amorphous semiconductor phase on the surface of a single crystal. Other liquid quenching techniques always had produced the stable crystalline Si phase. We have used this quenching technique to study glass formation in low-B Fe-B alloys.

The major problems in studies on metallic alloys are:

(i) ensuring the homogeneity of the melt obtained from a multiphase crystalline alloy, due to its short lifetime. Experiments with [illegible] experiments on Si (8) and heat-flow calculations (7) indicate that the lifetime of the melt is about 1 nsec. Since the thermal conductivity and optical absorption length for a metal are similar to those of the Si experiments on Si, a similar melt lifetime is expected. Since the atomic diffusivity in the melt is about $10^{-4}cm^2sec^{-1}$, the mixing length $\sqrt{Dt}$ is about 30Å. The starting material should therefore be homogeneous on this scale.

(ii) determining the structure of the ≤1000Å thick transformed layer. Unlike in the Si case, where is a reflectivity difference between the amorphous and crystalline phase, which allows convenient characterization by optical microscopy, the metals require direct diffraction methods for structural determination. Transmission electron microscopy (TEM) is clearly the technique of choice here. Since the rapid cooling requires a cold substrate that is much thicker than the 1000Å melt-depth, a problem arises in obtaining a thin foil for TEM observation. Thinning from the back is not an entirely satisfactory solution, since it does not permit investigation of an entire 100 μm diameter spot. We have developed a very satisfactory solution to both these problems, based on compositionally modulated films [illegible] as described below. It has the additional advantages of permitting a large number of samples with different compositions to be made from just two sputtering targets.

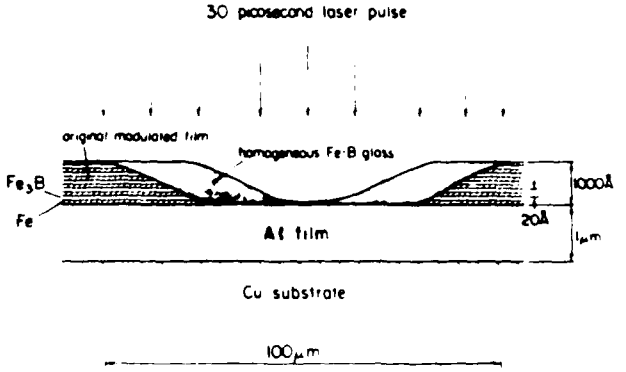

Figure 1 - Schematic cross-section, drawn to a variable scale, of a compositionally modulated film after irradiation by a 30 psec laser pulse with a Gaussian intensity profile.

Experimental Procedure

Fe $Fe_{76}B_{24}$ compositionally modulated films with modulation wavelengths of the order of the mixing length (~3Å) during the lifetime of the melt, were prepared by biased D.C. sputter-deposition from alternating targets of Fe and $Fe_{76}B_{24}$ (11). The films, about 1000Å thick, were deposited onto a water-cooled copper substrate coated by an evaporated Al film, as shown in Figure 1. The average composition of the films could most reliably be obtained from the independently obtained deposition rates of Fe and $Fe_{76}B_{24}$, and could be conveniently varied by adjusting the Fe $Fe_{76}B_{24}$ thickness ratio. Alloys with average composition in the range 0-24 at.%B were prepared.

The samples were irradiated with 30 psec Nd:YAG (λ = 1.06 μ) laser pulses, with a beam diameter of about 100 μm and an average fluence of [illegible] J/cm^2. The films were then taken off the substrates by dissolving the Al layer in a dilute NaOH solution, and could immediately be examined by transmission electron microscopy (TEM). This technique allows examination of a whole irradiated spot.

Results and Discussion

In the modulated films, the as-deposited Fe layers consisted of polycrystalline α-Fe with grain size less than 100Å (Figure 2(a)), and the as-deposited $Fe_{76}B_{24}$ layers were amorphous, as shown by the weak halo superimposed on the first ring of α-Fe diffraction patterns in Figure 2(b).

All the Fe-B alloys, with 24, 19, 15, 10, 8 and 5 at.% B, were found to form glasses after irradiation, as shown in Figure 2(c) and (d). Except for the 5 at.% B films, no epitaxial growth from the pre-existing α-Fe crystals or nucleation of metastable crystalline phases could be observed anywhere in the laser-irradiated spots. Films containing only 5 at.% B contained some large (~1000Å) bcc crystals at the edges of the irradiated regions, as shown in Figure 3(a) and (b). Although the lattice spacing is close to that of

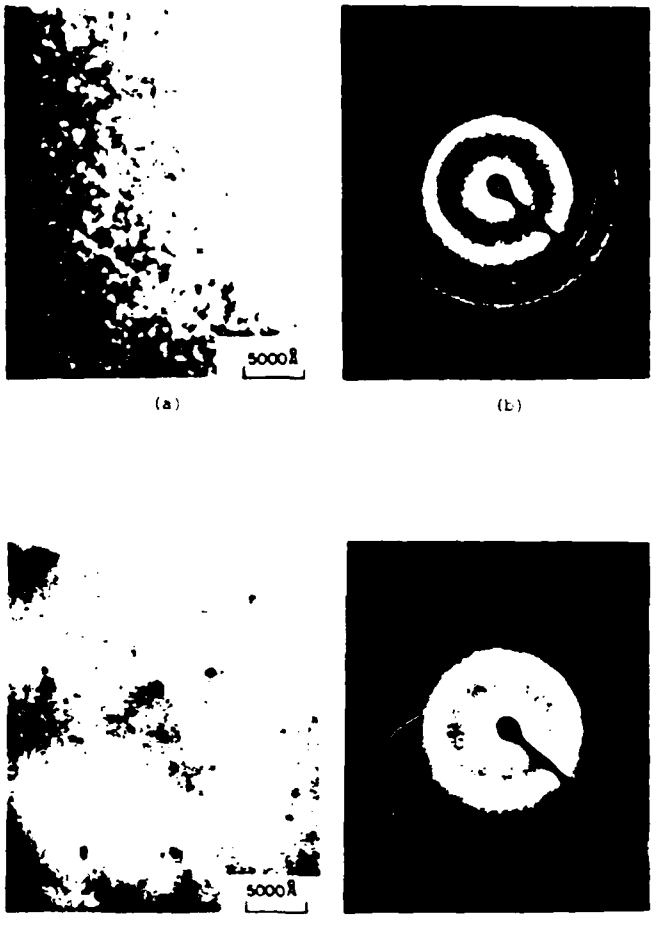

Figure 2 - TEM dark field images and the corresponding diffraction patterns from a $Fe_{95}B_5$ film before (a,b) and after (c,d) laser irradiation.

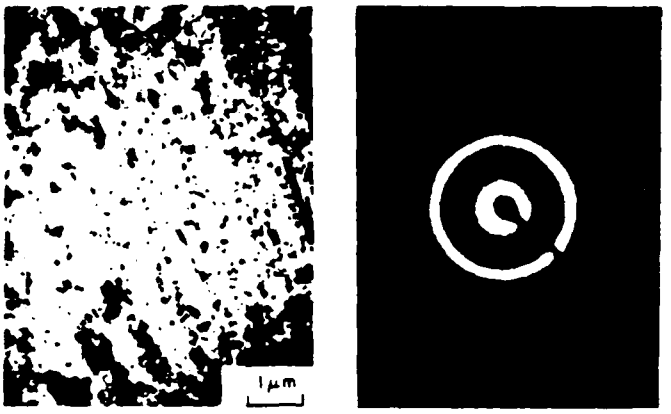

Figure 3 - TEM dark field image and corresponding diffraction pattern taken from the edge of a laser-irradiated spot on a $Fe_{95}B_5$ film.

α-Fe, it was not possible to determine whether the crystals consisted of α-Fe or a metastable $Fe_{95}B_5$ bcc solid solution, since the difference in lattice spacing between them is very small (~0.003Å)(6). Most likely they are $Fe_{95}B_5$, since growth of α-Fe crystals to such size would require diffusion over a distance of about 1000Å, which seems not possible during the short lifetime of the melt. These bcc crystals are present only at the edges of the irradiated spots. Their absence from the center of the spots rules out that they would be the result of homogeneous or heterogeneous nucleation in the melt. This leaves only epitaxial crystal growth as their possible origin. Since the lattice spacing of the metastable bcc $Fe_{95}B_5$ is very close to that of α-Fe, it is quite possible that the bcc $Fe_{95}B_5$ crystals grew epitaxially from the pre-existing α-Fe crystals that were present only at the edges of the irradiated spots (see Figure 1). In comparison, we notice that, after irradiation, no observable crystal growth occurred at the edges of the spots in the higher B-containing (>5 at.%) Fe-B alloys, whereas α-Fe crystals grew from the as-deposited grain size of 500Å to about 1 μm in pure Fe films (12). This indicates that B has a very strong effect on the crystal growth velocity of the Fe alloys. The change of driving force can also be a factor in some cases.

Since the time scale involved in this quenching method is so short, only partitionless solidification, either partitionless crystallization or glass formation, need to be considered. If partitionless crystallization can be prevented, a glass will be formed. In the low B-containing Fe-B alloys, the most obvious type of partitionless crystallization is the formation of metastable α-Fe(B) solid solutions.

It has been argued that the possibility of forming crystalline phase of the same composition as the melt makes glass formation difficult (13,14), since partitionless crystallization is thought usually to be a very fast process. In the Fe-B system, however, alloys with a B-content between 5 and

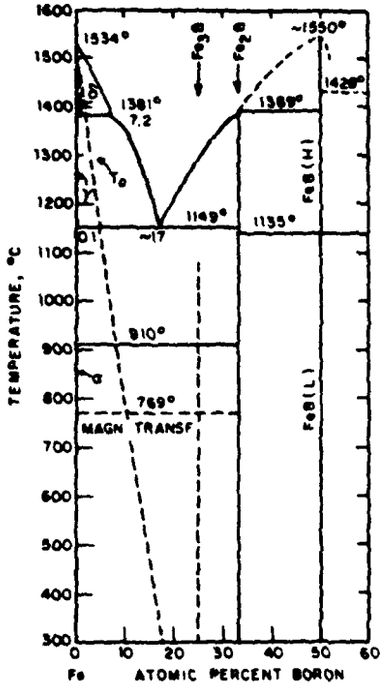

Figure 4 - Fe-B equilibrium phase diagram showing the T_0 line calculated by regular solution theory.

12 at.% can be quenched into glasses (at high quenching rates) as well as solid solutions (6) (at lower quenching rates). This indicates that, although partitionless crystallization is no doubt interface-limited, the kinetic coefficient is much smaller than the collision-limited value for pure elements (15,16), presumably due to the local rearrangements required to change the strong chemical short range order (17) around the B atom in the liquid state to that characteristic of the bcc solid solution (6). The same argument must also be invoked to account for the thermal stability of the glassy phase after the quench.

Figure 4 shows the calculated T_0 line of a solid α-Fe(B) solution with respect to a liquid Fe(B) solution. Regular solution behavior was assumed for both liquid and solid solutions in this calculation. The values of the exchange energy parameters at each temperature T were determined from the corresponding solidus and liquidus points at that temperature(18), and were then used to determine the corresponding composition on the T_0 line. The T_0 line can be regarded as the locus of the congruent melting points of the metastable α-Fe(B) solid solutions. Apparently, the congruent melting temperature is strongly depressed by adding B to Fe. This enhances the glass-forming ability, provided that glass transition temperature is a slowly varying function of composition. The observation that 12 at.% B-containing Fe-B

alloys can be quenched into single phase bcc solid solution suggested that T_o at 12 at.% B should be greater than the glass transition temperature. Our calculation is indeed in agreement with this speculation. Hasegawa et al. (5) observed that Fe-B glasses with about 18 at.% B or less crystallize first to the single phase bcc solution on heating. Our calculation shows that the composition corresponding to $T_o = T_c$ is about 16 at.%B, (T_c : crystallization temperature of the glass, 660K for 18 at.% B glass (5)) in good agreement with the observations, taking into account the approximate nature of the regular solution calculation.

Although for the 5-12 at.% B-containing Fe-B alloys, the T_o line lies above the glass transition temperature, these alloys can still be quenched into glasses (i.e.: not crystallize into bcc solutions) probably because of the drastic change in chemical short range order in the transition from liquid Fe(B) to a bcc α-Fe(B) solution. Since in none of the specimens crystal growth due to heterogeneous or homogeneous nucleation inside the melt was observed it is possible that Fe-B alloys with even lower B content can be quenched into glasses by this technique. This possibility is now being investigated.

Conclusion

We have demonstrated that the ultrahigh cooling rate induced by psec laser pulse irradiation can be used to obtain glassy Fe-B alloys with a B-content as low as 5 at.%, which is very significantly lower than the B-content required for glass formation by other liquid quenching techniques. The cooling rates in these experiments are the highest ones used so far to quench metallic liquid alloys, and the results illustrate the potential of the technique for formation of new glasses and for the study of the kinetics of crystal growth.

Acknowledgements

The authors thank Dr. J.M. Liu for his help in the operation of the laser and Prof. D. Turnbull for helpful discussions. This research was supported in part by the National Science Foundation, Materials Research Laboratory (DMR80-20247). C.J. Lin acknowledges support by a predoctoral fellowship from the Exxon Corporation.

References

1. W. Klement, R.H. Willens, and P. Duwez, "Non-crystalline Structure in Solidified Gold-Silicon Alloys", Nature ,187 (1960) pp. 869-870.
2. M.H. Cohen and D. Turnbull, "Molecular Transport in Liquids and Glasses", J. Chem. Phys., 31 (1959) pp. 1164-1169.
3. D. Turnbull, "Under What Conditions Can a Glass be Formed?", Contemp. Phys., 10 (1969) pp. 473-488.
4. H. Jones, "Effects of Experimental Variables in Rapid Quenching from the Melt", pp. 1-28 in Proc. 2nd Int. Conf. on Rapidly Quenched Metals, eds. N.J. Grant and B.C. Giessen (M.I.T. Press, Cambridge,Ma 1976).
5. R. Hasegawa and R. Ray, "Iron-Boron Metallic Glasses", J. Appl. Phys., 49 (1978) pp. 4174-4179.
6. R. Ray and R. Hasegawa, "Rapidly Quenched Metastable Iron-Boron Solid Solutions", Solid State Commun., 27 (1978) pp. 471-474.
7. N. Bloembergen, "Fundamentals of Laser-Solid Interactions", pp. 1-10 in 'Laser-Solid Interactions and Laser Processing', eds. S.D. Ferris, H.J. Leamy and J.M. Poate (AIP, New York 1979).

8. P.L. Liu, R. Yen, N. Bloembergen and R.T. Hodgson., "Picosecond Laser-induced Melting and Resolidification Morphology on Si", Appl. Phys. Lett. 34 (1979) pp. 864-666.
9. J.M. Liu, Thesis, "Thermal Model of Picosecond Laser Interactions with Silicon", Harvard University, 1982.
10. C.J. Lin and F. Spaepen, "Fe-B Glasses Formed by Picosecond Pulsed Laser Quenching", Appl. Phys. Lett., 1982 (in press).
11. A.L. Greer, C.J. Lin and F. Spaepen, "Pd-Fe Interdiffusion in Sputtered Amorphous Alloys", Proc. 4th Int. Conf. on Rapidly Quenched Metals, eds. T. Masumoto and K. Suzuki, (Japan Institute of Metals, 1982) pp. 567-572.
12. With the 1 nsec lifetime of the melt, this would give an average crystal growth velocity as high as 500 m/sec.
13. W.J. Boettinger, "The Effect of Alloy Constitution and Crystallization Kinetics on the Formation of Metallic Glass" pp. 99-102, in Proc. 4th Int. Conf. on Rapidly Quenched Metals, eds. T. Masumoto and K. Suzuki (Japan Institute of Metals, 1982) Vol. I.
14. T.B. Massalski, "Relationships between Metallic Glass Formation and Phase Diagrams", pp. 203-208, in Proc. 4th Int. Conf. on Rapidly Quenched Metals, eds. T. Masumoto and K. Suzuki (Japan Institute of Metals, 1982) Vol. I.
15. F. Spaepen and D. Turnbull, "Kinetics of Motion of Crystal-Melt Interfaces" pp. 73-83 in 'Laser-Solid Interactions and Laser Processing', eds. S.D. Ferris, H.J. Leamy and J.M. Poate (AIP, New York, 1979).
16. F. Spaepen and D. Turnbull, "Crystallization Process" in 'Laser Annealing of Semiconductors', eds. J.M. Poate and J.M. Mayer, Academic Press, NY 1982, Chapter 2, in press.
17. J.J. Gilman, "Structures of Ferrous Eutectic Liquids", Phil. Mag., B37 (1978) pp. 577-584. Also indicated by the large negative value we obtained for the exchange energy parameter in the liquid Fe(B) solution in the calculation of the T_c-line of Figure 4.
18. Below the eutectic temperature and in the γ-Fe region, an extrapolation of the solidus and liquidus lines was used.

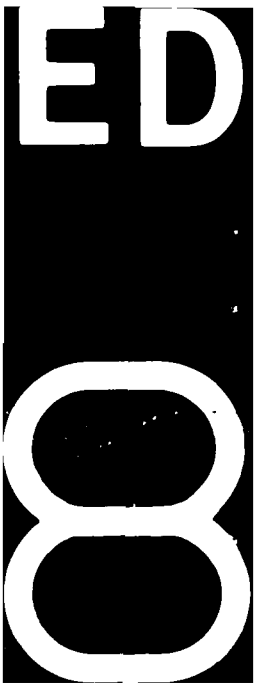
ED
8